Interaction between vortices and impurities in a d-wave superconductor

by

Avid Farhoodfar

A THESIS SUBMITTED IN PARTIAL FULFILMENT OF
THE REQUIREMENTS FOR THE DEGREE OF

MASTER OF SCIENCE

in

The Faculty of Mathematics and Sciences

Department of Physics

BROCK UNIVERSITY

March 16, 2005

In presenting this thesis in partial fulfilment of the requirements for an advanced degree at the Brock University, I agree that the Library shall make it freely available for reference and study. I further agree that permission for extensive copying of this thesis for scholarly purposes may be granted by the head of my department or by his or her representatives. It is understood that copying or publication of this thesis for financial gain shall not be allowed without my written permission.

(Signature) _____

Department of Physics

Brock University
St.Catharines, Canada

Date _____

Abstract

High temperature superconductors were discovered in 1986, but despite considerable research efforts, both experimental and theoretical, these materials remain poorly understood. Because their electronic structure is both inhomogeneous and highly correlated, a full understanding will require knowledge of quasiparticle properties both in real space and momentum space.

In this thesis, we will present a theoretical analysis of the scanning tunneling microscopy (STM) data in BSCCO. We introduce the Bogoliubov-De Gennes Hamiltonian and solve it numerically on a two-dimensional 20× 20 lattice under a magnetic field perpendicular to the surface. We consider a vortex at the center of our model. We introduce a Zn impurity in our lattice as a microscopic probe of the physical properties of BSCCO. By direct numerical diagonalization of the lattice Bogoliubov-De Gennes Hamiltonian for different positions of the impurity, we can calculate the interaction between the vortex and the impurity in a d-wave superconductor.

Contents

List of Figures

Chapter 1

Introduction

After the discovery of superconductivity in mercury at 4K in 1911 by the Dutch physicist H. Kamerlingh-Onnes, a rush of interest led to the discovery of many other superconductors, mostly pure elements or simple alloys. Fig. 1.1 shows the transition temperatures of some superconductors and the year of discovery. Superconductivity seemed like a great technological tool, but the temperature needed to operate even the highest T_c superconductor was prohibitively expensive to attain, because one needs liquid helium.

In 1973, the "record high" for a superconducting phase transition temperature was $T_c \approx 23.3$K for Nb_3Ge, and it was widely felt that this value of T_c could at best be improved by only a degree or two in some exotic metallic alloys. A very important breakthrough came in 1986 with the observation by Bednorz and Müller of superconductivity at around 30K in "LBCO"(a mixed oxide of lanthanum, barium and copper). By 1987, a compound of yttrium, barium, copper, and oxygen ("YBCO") had been discovered with $T_c > 77$ K, the boiling point of liquid nitrogen. This increase has enormous significance, because it means that superconducting materials are now accessible at liquid nitrogen temperatures. Cooling by liquid nitrogen is considerably cheaper than cooling by liquid helium.

Unlike the simple conventional superconductors, high T_c superconductors have complex layered structures. In all high T_c superconductors, the superconductivity is a product of the copper-oxide (CuO_2) layer. Adjacent sets of n Cu-O planes are separated from the next set of n Cu-O planes by charge reservoir layers, or metal-O isolation layers, which controls the oxidation state of copper ions, where metal atoms usually are La, Ba, Tl or Bi. While these reservoir layers may differ in different materials, this CuO_2 layer is a feature of most high T_c superconductors, Fig. 1.2 [1].

Even a decade and a half after the discovery of high T_c superconductors, these materials continue to puzzle condensed-matter theorists. Depending on the temperature and the level of doping, the

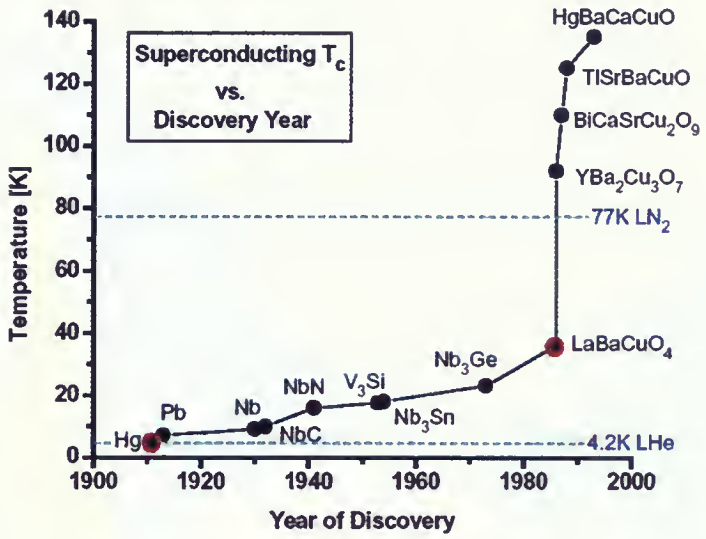

Figure 1.1: Highest T_c discovery history. (Points circled in grey garnered a Nobel Prize for their discoverers: Kamerlingh-Onnes in 1913 and Bednorz & Müller in 1987.)

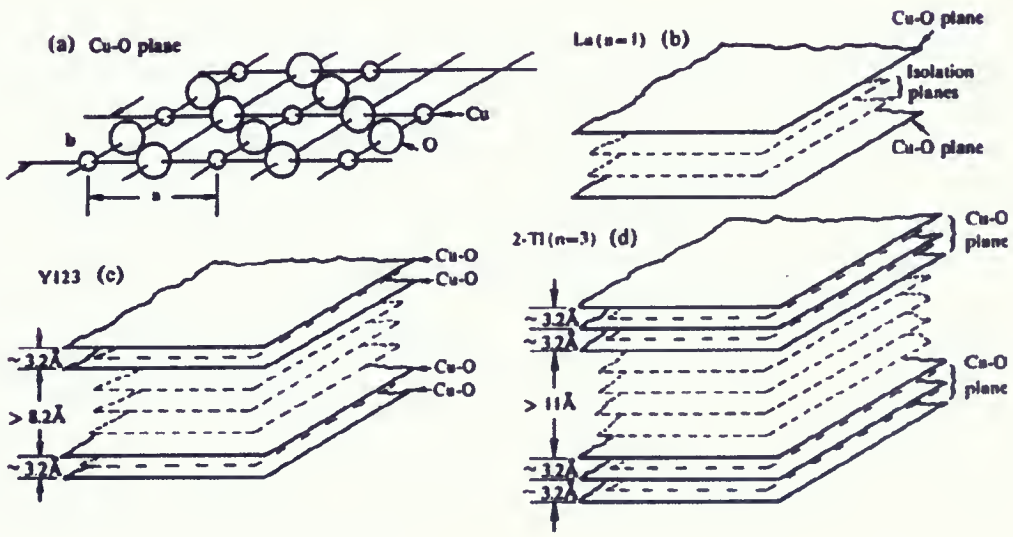

Figure 1.2: (a) An infinite planes of Cu-O atoms. (b) Cu-O planes in $La_{2-x}Sr_xCuO_4$. (c) Cu-O planes in $YBa_2Cu_3O_{7-\delta}$. (d) Cu-O planes in $Tl_2Sr_2Ca_2Cu_3O_10$ [1].

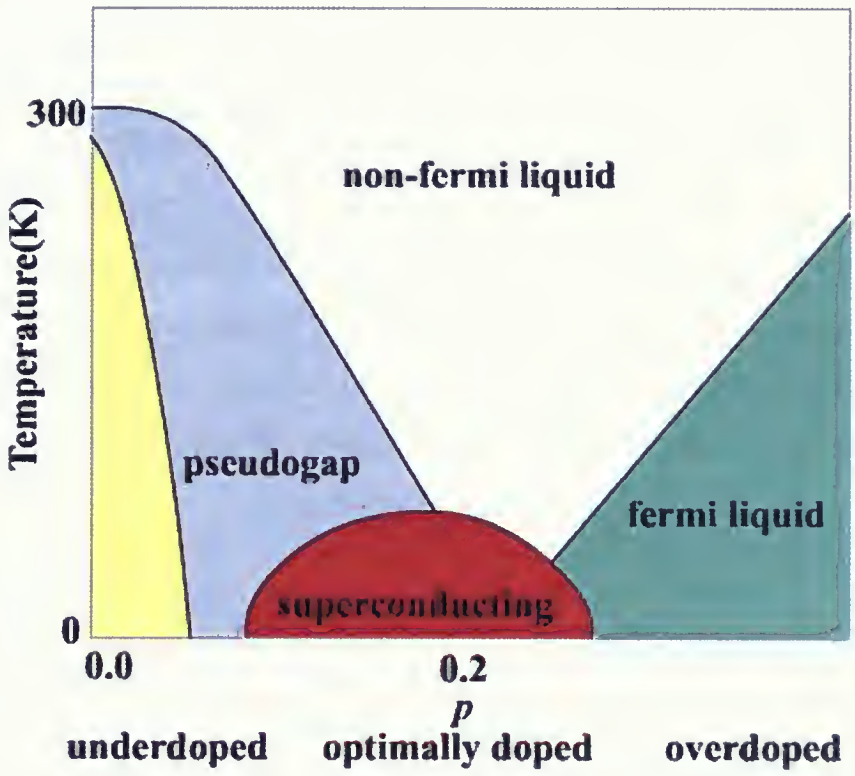

Figure 1.3: The electronic phase diagram of the HTSC

cuprates can be insulators, metals or superconductors, see Fig. 1.3. Extensive research to find high-temperature superconductivity in other families of materials, has been singularly unsuccessful.

A common feature of all superconductors both the low and the high-temperature variety is that the electrons somehow overcome their mutual electrostatic repulsion to form "Cooper pairs". An electron has a spin of 1/2 and thus the total spin of cooper pair can be either 0 or 1. In a singlet Cooper pair, the electron spins (+1/2 or -1/2) cancels and the total spin is 0. In a triplet pair, the total spin is 1. In this work we only consider the singlet Cooper pairs relevant for HTSC. Since the Cooper pairs are bosons and therefore do not have to obey the Pauli exclusion principle, they can condense into a single quantum state below a certain temperature. This is what gives superconductors their unusual properties.

In low-temperature superconductors the electrons pair together so that their total orbital angular momentum is zero, a so-called s-wave state. Interactions between the electrons and phonons (vibrations of the crystal lattice) are responsible for the pairing. The electronic states of Cooper

pairs in high T_c superconductors are markedly different from those in conventional ones: the two electrons revolve around each other much faster and farther apart. These wider orbits are analogous to the higher-energy d-orbital of electrons around an atom, and high T_c superconductors are often called d-wave superconductors.

The superconducting properties are qualitatively modified by impurity atoms, depending, for example on whether they are magnetic or non-magnetic. In principle, this analysis can be useful as a method of identifying the nature of the pairing state in superconductors. In this thesis we consider the effect of a single point-like non-magnetic impurity, Zn, in a d-wave superconductor.

1.1 Overview

The thesis is organized as follows. Chapter 2 details the general properties of conventional superconductors as well as unconventional ones. We will briefly discuss the effect of magnetic field on a superconductor, the different types of superconductors and the vortex state. Then we talk about the Ginzburg-Landau equation and the BCS theory of superconductivity, then the pairing mechanism in superconductors, t-J model, the Bogoliubov-De Gennes Hamiltonian, and the effect of impurities on superconductors. Chapter 3 describes the measurements one can make with a scanning tunneling microscope. In addition, it summarizes some results of the STM studies on BSCCO. Chapter 4 describes the model we have developed, and the computational details of the numerical diagonalization of the lattice Bogoliubov-De Gennes Hamiltonian, and addresses some of the numerical difficulties which arise due to the open boundary condition. Finally, Chapter 5 summarizes the results and presents the conclusions arising from the calculation of the interaction between vortices and impurities in a d-wave superconductor.

Chapter 2

Reveiw of the superconductivity

In this chapter we review some of the basic facts about superconductors. We focus on the magnetic response and impurity effects.

2.1 Introduction

Superconductivity is the name given to a remarkable combination of electric and magnetic properties which appears in certain metals when they are cooled to extremely low temperatures. Superconductors have two distinguishing properties. The obvious one is zero resistivity. However, superconductors are more than just materials which are perfectly conducting. Inside a perfect metal there may or may not be a non-zero magnetic induction $\mathbf{B}$, depending on circumstances. Superconductors do not allow magnetic field to penetrate them the way normal materials do, i.e. inside a superconducting metal we always have $\mathbf{B} = 0$, which shows that the superconductors are perfect diamagnets. In particular, when superconductors are cooled below a critical temperature T_c in the presence of an externally applied magnetic field, all of the magnetic flux is expelled from their interior. When the external field exceeds a critical value (H_c), the superconductor returns to its normal state. This effect, whereby a superconductor never has a flux density inside, is called the Meissner effect. The Meissner effect can be understood using the Ginsburg-Landau (GL) theory.

2.2 Ginsburg-Landau theory

The GL theory uses quantum mechanics to predict the effect of magnetic field on superconductors. In this theory, the wave function of the Cooper Pairs $\psi(\mathbf{r})$ is introduced as a complex order parameter such that $|\psi(\mathbf{r})|^2$ presents the local density of superconducting electrons, $n_s(\mathbf{r})$. The theory is

developed by applying a variational method to an expansion of the free energy density in powers of $|\psi|^2$ and $|\nabla\psi|^2$, leading to a pair of differential equations for $\psi(\mathbf{r})$ and the vector potential $\mathbf{A}(\mathbf{r})$.

The basic postulate of GL is if ψ is small, and varies slowly in space, the free energy of the superconducting electrons can be expanded in a series of the form [2]

$$F_s = F_n + \int F_{GL} d^3\mathbf{r}, \tag{2.1}$$

where F_n is the Gibbs free energy in the normal state, and F_{GL} in an external magnetic field $\mathbf{H}$ is

$$F_{GL} = \alpha|\psi|^2 + \frac{\beta}{2}|\psi|^4 + \frac{1}{4m}\left|\left(-i\hbar\nabla + \frac{2e}{c}\mathbf{A}\right)|\psi|^2 + \frac{\mathbf{B}^2}{8\pi} - \frac{\mathbf{B}\cdot\mathbf{H}}{4\pi}\right., \tag{2.2}$$

where $\alpha = a(T - T_c)$, and T_c is the superconducting critical temperature. We introduce

$$K = \frac{\hbar}{4m}, \tag{2.3}$$

and

$$\mathbf{D} = -i\nabla + i\frac{2e}{\hbar c}\mathbf{A}. \tag{2.4}$$

By using (2.3) and (2.4) we can write (2.2) as

$$F_{GL} = \alpha|\psi|^2 + \frac{\beta}{2}|\psi|^4 + K|\mathbf{D}\psi|^2 + \frac{\mathbf{B}^2}{8\pi} - \frac{\mathbf{B}\cdot\mathbf{H}}{4\pi}. \tag{2.5}$$

If $\psi = 0$, (2.5) reduces to the free energy of the normal state $F_n = \mathbf{B}^2/8\pi - \mathbf{B}\cdot\mathbf{H}/4\pi$. The three remaining terms describe superconducting effects.

If ψ is constant, (2.5) reduces to the London free energy in an applied magnetic field $\mathbf{H}$ [2]. In the absence of fields and gradients, we have $F_s - F_n = \alpha|\psi|^2 + \frac{1}{2}\beta|\psi|^4$, which can be viewed as a series expansion in powers of $|\psi|^2$ or n_s, in which only the first two terms remain. If $T > T_c$, the minimum free energy occurs at $|\psi|^2 = 0$, corresponding to the normal state. When $T < T_c$, the minimum occurs when

$$|\psi|^2 = -\frac{\alpha}{\beta}. \tag{2.6}$$

The condensation energy by using the definition of the thermodynamic critical field H_c, is $F_s - F_n = -H_c^2/8\pi$. We can find the GL equations by minimizing the Gibbs free energy, F_s, in a given magnetic field $\mathbf{H}$. The first GL equation is the result of variation of F with respect to the order parameter $\psi(\mathbf{r})$,

$$\alpha\psi + \beta|\psi|^2\psi - K\mathbf{D}^2\psi = 0. \tag{2.7}$$

The second GL equation, which gives us a definition of the supercurrent, is the result of variation with respect to the vector potential $\mathbf{A}$,

$$\mathbf{J}_s = -i\frac{2e}{\hbar}K\left[(\mathbf{D}\psi)^*\,\psi - \psi^*\,(\mathbf{D}\psi)\right], \tag{2.8}$$

where we have used the Maxwell equation, $\nabla \times \mathbf{B} = (4\pi/c)\mathbf{J}$. By considering $\psi(\mathbf{r}) = |\psi(\mathbf{r})|e^{i\phi(\mathbf{r})}$ and using the definitions for K and $\mathbf{D}$, (2.8) becomes

$$\mathbf{J}_s = \frac{2e^2}{mc}|\psi|^2\left(-\frac{\hbar c}{2e}\nabla\phi - \mathbf{A}\right) = 2e|\psi|^2\mathbf{v}_s, \tag{2.9}$$

where we have used

$$\mathbf{v}_s = \frac{1}{2m}\left(\mathbf{p}_s - \frac{2e\mathbf{A}}{c}\right) = \frac{1}{2m}\left(\hbar\nabla\phi - \frac{2e\mathbf{A}}{c}\right).$$

The expression (2.8) has exactly the form of the quantum-mechanical expression for particles of mass $2m$, charge $2e$, and wavefunction $\psi(\mathbf{r})$. Apart from the nonlinear term, (2.7) has the form of Schrödinger's equation for such particles, with energy eigenvalue $-\alpha$. We define the correlation length, $\xi(T)$, as the characteristic length for variation of ψ by

$$\xi^2(T) = \frac{\hbar^2}{4m|\alpha(T)|} \propto \frac{1}{T_c - T}. \tag{2.10}$$

2.3 Type-I and type-II superconductors

Superconductors can expel magnetic fields from their interior in two different ways. In an applied magnetic field of strength H, the free energy per unit volume of the normal state is greater than that of superconducting, perfectly diamagnetic state, by an amount $(H_c^2 - H^2)/8\pi$. Furthermore, there is a surface energy associated with the boundary between a normal and superconducting region. For type-I superconductors surface energy is positive. Hence, if energy increases on normal region, there would be an increase in free energy due to both the bulk and the surface of the normal region. For this reason, type-I superconductor remains superconducting throughout when a magnetic field less than H_c is applied [3]. Type-I superconductors allow no magnetic field at all to penetrate their interior. The shielding currents exist only near the surface. However, if the external magnetic field is too strong, the superconductor cannot shield it without surpassing its own critical current. Magnetic fields larger than H_c, will destroy the superconductivity in the material.

In type-I superconductors, the surface energy is positive because the penetration depth λ_L, the characteristic range of magnetic field into the superconductor, is shorter than the coherence length ξ. So the Ginzburg-Landau parameter κ ($\kappa \equiv \lambda_L/\xi$) is $\kappa < 1$.

In some materials the surface energy between normal and superconducting regions is negative. It is possible if the coherence length ξ is shorter than the penetration depth λ_L, and therefore the appearance of normal region would reduce the free energy, if the increase in free energy due to the bulk of the region were outweighed by the decrease due to the surface. When the magnetic field is applied, a large number of normal regions would form in the superconducting material. The material would split into some fine-scale mixture of superconducting and normal regions, as is shown in Fig. 2.1. These materials are type-II superconductors. High T_c superconductors (we will discuss them later) are type-II superconductors.

Type-II superconductors, like type-I superconductors, allow no magnetic field to penetrate their interior below a lower critical field H_{c1}. However, Abrikosov showed that for $\kappa > 1/\sqrt{2}$, what is called mixed state or vortex state is formed. In this state, for magnetic fields, $H_{c1} < H < H_{c2}$, Abrikosov vortices occur in the superconductor. At the center of a vortex, the superconducting order parameter reaches zero.

For type-II superconductors in an applied magnetic field, finding the highest field at which superconductivity can nucleate in the interior of a large sample, H_{c2} is equivalent to quantum harmonic oscillator problem for a particle of mass $2m$ bound in a harmonic oscillator potential with force constant $(2\pi\hbar H/\Phi_0)^2/2m$. This is the same problem as finding the quantized states of a normal charged particle in a magnetic field

$$\epsilon_n = \left(n + \frac{1}{2}\right)\hbar\omega_c = \left(n + \frac{1}{2}\right)\hbar\left(\frac{2eH}{2mc}\right). \tag{2.11}$$

By using (2.10), the corresponding value is defined as $H_{c2} = \Phi_0/2\pi\xi^2(T)$, where Φ_0 is the total flux.

2.4 Vortices

When the first flux enters the type-II superconductor, it is carried by an array of vortices sparsely distributed through the material. As long as the separation is large compare to λ_L, the vortices

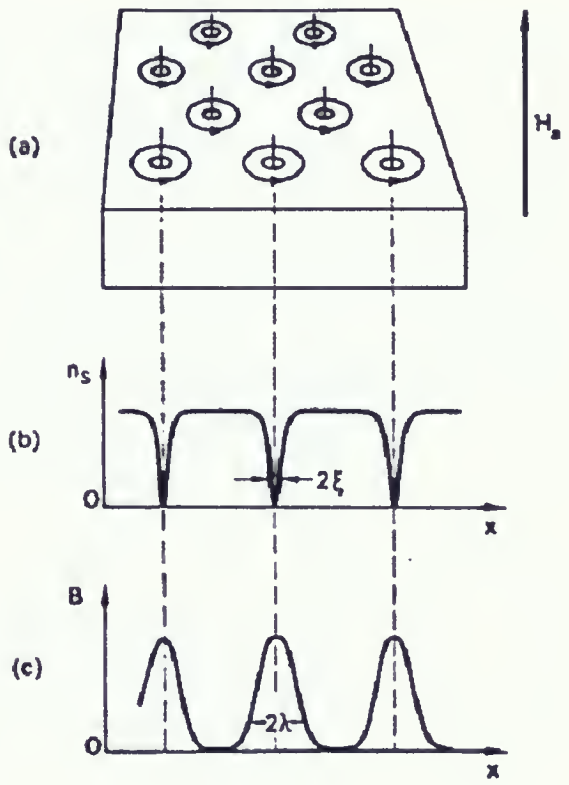

Figure 2.1: Mixed state in an applied magnetic field just above H_{c1}. (a) Lattice of cores and associated vortices. (b) Variation with position of concentration of superelectrons. (c) Variation of the magnetic induction.

would not interact or overlap, so that each can be treated in isolation. By finding the self-consistent solution of the GL equations for $\psi(\mathbf{r})$ and $\mathbf{B}$ by using the axial symmetry, one can find the free extra energy ϵ_1 per unit length of the line. This determines H_{c1} in following manner. When $H = H_{c1}$ the Gibbs free energy, by definition must have the same value whether the first vortex is in or out of the sample. The Gibbs free energy, G, is the thermodynamic potential for constant H. In superconducting state we have

$$G_s = V f_s - \frac{V_{ext} H_a^2}{8\pi}. \tag{2.12}$$

Thus at H_{c1}

$$G_s|_{no\ flux} = G_s|_{first\ vortex}.$$

Since $G = F - (H/4\pi)\int B d\mathbf{r}$, $G_s = F_s$ in the absence of flux, and the condition becomes

$$F_s = F_s + \epsilon_l L - \frac{H_{c1}\int B d\mathbf{r}}{4\pi} = F_s + \epsilon_l L - \frac{H_{c1}\Phi_0 L}{4\pi},$$

where L is the length of the vortex line in the sample. Therefore

$$H_{c1} = \frac{4\pi\epsilon_l}{\Phi_0}. \tag{2.13}$$

The calculation of ψ, $\mathbf{B}$ and ϵ_l for any κ requires a numerical solution of GL equations. It is convenient to introduce a vortex wavefunction as

$$\psi = \psi_\infty f(r) e^{i\theta}, \tag{2.14}$$

which builds the axial symmetry and the fact that the phase of ψ varies by 2π in making a complete circuit, corresponding to the existence of a single flux quantum associated with the vortex. This phase choice for ψ fixes the gauge choice for $\mathbf{A}$ so that

$$\mathbf{A} = A(r)\hat{\Theta}, \tag{2.15}$$

with

$$A(r) = \frac{1}{r}\int_0^r r'\mathbf{B}(r')dr'. \tag{2.16}$$

When we solve GL equation [2] the exact solution for $\mathbf{B}$ is

$$\mathbf{B}(r) = \frac{\Phi_0}{2\pi\lambda_L^2} K_0(\frac{r}{\lambda_L}),$$

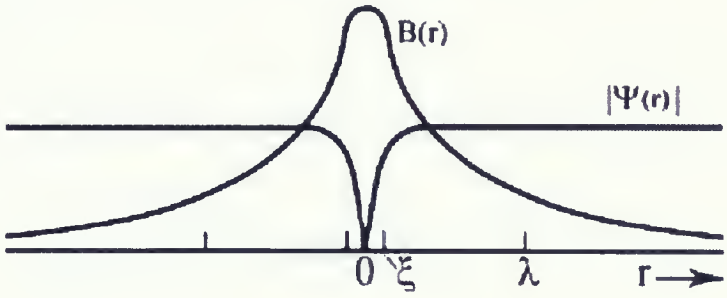

Figure 2.2: A single vortex is characterized by the presence of a magnetic field B(**r**), which peaks at its center and decreases on the length scale of the penetration depth λ_L. It is also characterized by a destruction of the superconducting order parameter $|\psi(\mathbf{r})|$ at its center, which recovers over the length scale of the coherence length ξ.

where K_0 is the zeroth-order Hankel function of imaginary argument. Quantitatively, $K_0(r/\lambda_L)$ cuts off at e^{-r/λ_L} at large distance and diverges logarithmically as $\ln(\lambda_L/r)$ as $r \to 0$. In reality this divergence is cut off at $r \approx \xi$, where $|\psi|^2$ starts dropping to zero. Therefore, $\mathbf{B}(r)$ is actually regular at the center of the vortex, as shown in Fig. 2.2. Finally, we note that at $\lambda_L \gg \xi$, the magnetic field can be assumed to be uniform (except near the lower critical field H_{c1}).

2.5 Cooper pairs and BCS theory

The first great difficulty in the development of the theory of superconductivity was to discover the nature of the interaction responsible for the transition to superconductivity. The first widely-accepted theory to explain superconductivity put forth in 1957 by John Bardeen, Leon Cooper, and John Schriefer. Cooper assumed a non-interacting Fermi gas at 0 K, all states are filled by $k \leq k_F$, and he added two electrons to the system. They occupy states with $k > k_F$ because of Pauli exclusion principle. He showed that even if both electrons are restricted to having momenta outside the Fermi sphere, they will have a bound state lying below $2E_F$. This bound state is called Cooper pair. Fermi sea is unstable against the formation of a bound Cooper pair when the net interaction is attractive, in other word pairs condense until an equilibrium point is reached. Cooper pairs are the basis of BCS theory. The "BCS theory of superconductivity" is widely applicable, from ^{3}He atoms

in their condensed phase, to type I and type II metallic superconductors, and is believed it can be useful for studying high T_c superconductors. The theory asserts that, as electrons pass through a crystal lattice, the lattice deform inward towards the electrons, generating phonons. These phonons produce a thorough of positive charge in the area of deformation that assist subsequent electrons in passing through the same region in a process known as phonon-mediated coupling.

BCS considered the Hamiltonian

$$\mathcal{H}_{BCS} = \sum_{\mathbf{k}\sigma} \epsilon_{\mathbf{k}} c^{\dagger}_{\mathbf{k}\sigma} c_{\mathbf{k}\sigma} + V \sum_{\mathbf{k}} c^{\dagger}_{\mathbf{k}\uparrow} c^{\dagger}_{-\mathbf{k}\downarrow} c_{-\mathbf{k}\downarrow} c_{\mathbf{k}\uparrow}, \tag{2.17}$$

where V is the attractive pairing potential and assumed to be non-zero within a thin shell over Fermi surface of thickness $\epsilon_l << \epsilon_F = \hbar^2 k_F^2/2m$ in momentum space. In BCS theory the "anomalous averages" $< c_{\mathbf{k}\uparrow} c_{-\mathbf{k}\downarrow} >$ and $< c^{\dagger}_{\mathbf{k}\uparrow} c^{\dagger}_{-\mathbf{k}\downarrow} >$, which are zero in normal metal, become finite in superconducting state. It is natural to define the order parameter of the superconducting state, Δ, as

$$\Delta = V \sum_{\mathbf{k}} < c_{\mathbf{k}\uparrow} c_{-\mathbf{k}\downarrow} > . \tag{2.18}$$

The BCS wavefunction is

$$|\Psi_{BCS}\rangle = \prod_{\mathbf{k}} \left[u(\mathbf{k}) + v(\mathbf{k}) c^{\dagger}_{\mathbf{k}\uparrow} c^{\dagger}_{-\mathbf{k}\downarrow} \right] |0\rangle, \tag{2.19}$$

where $|0\rangle$ is the vacuum state. The quantities $u(\mathbf{k})$ and $v(\mathbf{k})$ must be chosen to minimize the free energy and are not independent, but are fixed by normalization of the BCS wavefunction. v_k^2 is the propapility that the momentum pair state is full and u_k^2 is the probability that it is empty.

One of the predictions of BCS theory is that there is an energy gap in the allowed state about E_F, of the order of $k_B T_c$. BCS calculate the 0K energy gap, 2Δ, to be [2]

$$2\Delta = \frac{\hbar\omega_c}{\sinh[1/N(E_F)V]} \approx 4\hbar\omega_c e^{-1/N(E_F)V}. \tag{2.20}$$

The idea of the gap in the density of states is shown in Fig. 2.3. The normal state is shown, which at zero-temperature is filled up to E_F. For superconductors the zero-temperature gap is centered at E_F and it pushes allowed states into energy regions just below and above the gap. The Fermi energy may be taken as zero and the modified superconducting density of states, $N_S(E)$, for $E > \Delta$ and $E < -\Delta$, is

$$N_S(E) = N(0) \frac{E}{(E^2 - \Delta^2)^{1/2}}. \tag{2.21}$$

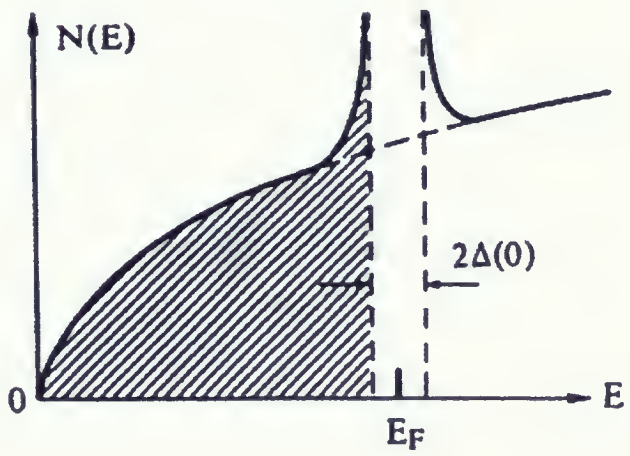

Figure 2.3: Density of states is filled with electrons up to E_F and the superconducting energy gap 2Δ.

For energies within the gap, the density of allowed states is zero. It is singular at the edge of the gap ($E = \pm\Delta$). The wave function of a pair is unchanged if the positions of the electrons are exchanged. This immediately implies that the spin part of the wave function is antisymmetric in accordance with the Pauli exclusion principle. In particular, the electron pairs are in a spin-singlet state $S = 0$ with antiparallel spins. The pairing mechanism in a conventional superconductor is thus appropriately called, s-wave spin-singlet. The energy gap of an s-wave superconductor is finite over the entire Fermi surface. Under ideal circumstances, the magnitude of the gap is the same at all points on the Fermi surface. BCS theory assumes the Fermi surface is spherical (Fig. 2.4) and $k_F^2 = k_x^2 + k_y^2$. While attractive interaction arises from the electron-phonon interaction, many non-phonon pairing mechanisms have been suggested the high T_c materials.

In this work, we consider quasiparticle properties in presence of vortices on a lattice. The appropriate starting point is the system of normal electrons on a lattice, which is analyzed using the band theory.

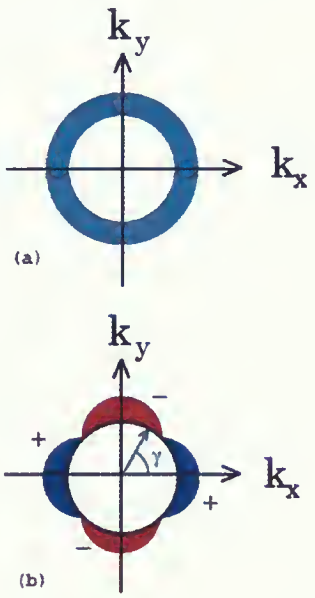

Figure 2.4: a) Fermi surface for s-wave superconductors. b) Fermi surface for d-wave superconductors.

2.6 Band theory

Band theory explains how electrons move in solids. Most simple metals (e.g. Cu, Ag, Au, etc.) and conventional superconductors contain conduction electrons that extend over many unit cells, and their wavefunctions can be approximated by Bloch waves. This leads to the electronic bands in the **k**-space. Starting with the free electron idea and adding the atomic cores with their translational symmetry, the energy $\epsilon(\mathbf{k})$ can be calculated, and this gives bands and what is usually called band theory [4].

A structurally dominating aspect of d-wave superconductors is the current carriers are considered to move in the copper-oxygen planes since the coupling between different layers is quite weak. For theoretical study, one usually uses a two-dimensional tight-binding model to describe the system [5].

2.6.1 The tight-binding approximation

One of the simplest models of electrons in solids is the tight-binding approximation. As free atoms are brought together, the Coulomb interaction between the atom cores and the electrons splits the energy levels, spreading them into bands. Each state of given quantum number of the atom is spread in the crystal into a band of energies. The width of the band is proportional to the strength of the overlap interaction between neighboring atoms. The approximation that starts out for the wave function of the free atoms is known as tight-binding approximation.

Suppose that the ground state of an electron of an insulated atom moving in the potential $U(r)$ is $\phi(r)$. If the influence of one atom on another is small, we obtain an approximate wavefunction for one electron

$$\psi_{\mathbf{k}}(r) = \sum_j C_{\mathbf{k}j}\phi(\mathbf{r} - \mathbf{r}_j), \tag{2.22}$$

where the sum is over all lattice points. The wavefunction (2.22) is of the Bloch form if $C_{\mathbf{k}j} = N^{-1/2}e^{i\mathbf{k}\cdot\mathbf{r}_j}$, where N is the number of atoms in the crystal [4]. We find the first-order energy by calculating the diagonal matrix elements of the Hamiltonian of the crystal:

$$\langle \mathbf{k}|H|\mathbf{k}\rangle = N^{-1}\sum_j\sum_m \exp\left[i\mathbf{k}\cdot(\mathbf{r}_j - \mathbf{r}_m)\right]\langle\phi_m|H|\phi_j\rangle\,, \tag{2.23}$$

where $\phi_m \equiv \phi(\mathbf{r} - \mathbf{r}_m)$. If we choose $\rho_m = \mathbf{r}_m - \mathbf{r}_j$, (2.23) becomes

$$\langle \mathbf{k}|H|\mathbf{k}\rangle = \sum_m \exp\left(i\mathbf{k}\cdot\rho_m\right)\int dV\phi^*(\mathbf{r} - \rho_m)H\phi(r). \tag{2.24}$$

Since we look just for the effect of the nearest neighbors, we can neglect all integrals in (2.24) except those on the same atom and those between nearest neighbors connected by ρ. We write

$$\int dV\phi^*(r)H\phi(r) = -t_0,$$

for the same atom and

$$\int dV\phi^*(r - \rho)H\phi(r) = -t_1,$$

for the nearest neighbors. The first-order energy, provided $\langle \mathbf{k}|\mathbf{k}\rangle = 1$ is

$$\langle \mathbf{k}|H|\mathbf{k}\rangle = -t_0 - t_1\sum_m \exp(-i\mathbf{k}\cdot\rho_m) = \epsilon_{\mathbf{k}}. \tag{2.25}$$

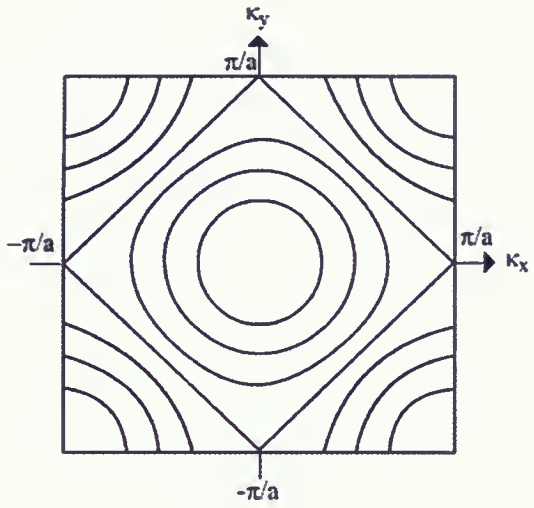

Figure 2.5: The Fermi surface of a tight binding model.

For a square lattice with lattice spacing a, the nearest neighbors are $\rho = (\pm a, 0)$ and $\rho = (0, \pm a)$ so the (2.25) will become

$$\epsilon(\mathbf{k}) = -t_0 - 2t_1(\cos k_x a + \cos k_y a).$$

If we assume the next-nearest-neighbor-hopping as well, we find that

$$\epsilon(\mathbf{k}) = t_0 - 2t_1 \left[\cos k_x a + \cos k_y a\right] - 4t_2 \cos k_x a \cos k_y a. \tag{2.26}$$

The Fermi surfaces for different ground state energies are shown in Fig. 2.5.

2.7 High temperature superconductivity

High-T_c superconductors, or HTSC, have high transition temperatures, accompanied by high critical current and magnetic fields. Being type-II, all high-T_c superconductors are in the vortex state for $H_{c1} < H < H_{c2}$. As described in previous section, when a type-II superconductor is placed in a magnetic field, quantized vortices are formed Fig. 2.2.

All HTSCs have layered structure, with parallel sheets of CuO_2 being the common structure feature. All these layer compounds are strongly anisotropic in electrical properties measured parallel or perpendicular to the layers. It is sometimes argued that cuprate superconductors are essentially

two-dimensional and they can be considered as a model with the effect of isolated CuO_2 planes. In most cuprates the Fermi level falls near three orbitals of the CuO_2 planes, the $3d_{x^2-y^2}$ orbital on Cu and overlapping $2p_x$ and $2p_y$ orbitals on two neighboring O atoms.

The properties of the cuprates are believed to be well explained by the two-dimensional Hubbard model. This model is tight-binding type with one atomic orbital per lattice site. The Hamiltonian is

$$H = -t \sum_{\mathbf{i,j},\sigma} c^{\dagger}_{i\sigma} c_{j\sigma} + U \sum_{\mathbf{i}} n_{i\uparrow} n_{i\downarrow}, \tag{2.27}$$

where i is the general site index, site j is the neighbor of site i and σ is a spin index. Many attempts have been made to simplify the Hubbard model. A good approximation is the t-J model, which explicitly includes mobile holes moving in presence of a background of antiferromagnetic spin correlations.

2.7.1 The t-J model

The t-J model Hamiltonian in represented by

$$H = H_0 + H_J, \tag{2.28}$$

where H_0 is defined by

$$H_0 = -\sum_{\mathbf{ij}} t_{ij}(1 - n_{i,-\sigma}) c^{\dagger}_{i\sigma} c_{j\sigma} (1 - n_{j,-\sigma}) - \mu \sum_{\mathbf{i}} c^{\dagger}_{i\sigma} c_{i\sigma}, \tag{2.29}$$

The factors $(1 - n_{i,-\sigma})$ are introduced to project out the states with double-occupied sites, i and j are sites of the square lattice, t_{ij} is nearest neighbor hopping amplitude defined as

$$t_{ij} = t \exp\left(\frac{ie}{\hbar c} \int_{R_i}^{R_j} \mathbf{A} \cdot d\mathbf{r}\right), \tag{2.30}$$

because of hermiticity we have $t_{ij} = t^*_{ij}$. The phase factor is known as "Peierls factor" and describes the magnetic field effects in the tight-binding model.

Below we analyse the origin of d-wave pairing, using a simplified version of (2.29), relaxing the no double-occupancy constraint [6]. If $\mathbf{A} = 0$ we will have

$$H_0 = -2t \sum_{\mathbf{ij}} c^{\dagger}_{i\sigma} c_{j\sigma} - \mu \sum_{\mathbf{i}} c^{\dagger}_{i\sigma} c_{i\sigma}. \tag{2.31}$$

H_J is defined by

$$H_J = J \sum_{\mathbf{ij}} \mathbf{S}_i \cdot \mathbf{S}_j, \tag{2.32}$$

where J is exchange coupling, and $\mathbf{S}_i$ is the spin-1/2 operator at a site i

$$\mathbf{S}_i = \frac{1}{2} c^\dagger_{i\sigma} \sigma_{\sigma\sigma'} c_{i\sigma}. \tag{2.33}$$

For antiferromagnetic interaction we have $J > 0$. By using (2.33) we calculate

$$\begin{aligned} \mathbf{S}_i \cdot \mathbf{S}_j &= S^x_i S^x_j + S^y_i S^y_j + S^z_i S^z_j \\ &= -\frac{1}{2}(c^\dagger_{i\uparrow} c^\dagger_{j\downarrow} - c^\dagger_{i\downarrow} c^\dagger_{j\uparrow})(c_{j\downarrow} c_{i\uparrow} - c_{j\uparrow} c_{i\downarrow}) \\ &\quad + \frac{1}{4}(c^\dagger_{i\uparrow} c_{i\uparrow} c^\dagger_{j\downarrow} c_{j\downarrow} + c^\dagger_{i\downarrow} c_{i\downarrow} c^\dagger_{j\uparrow} c_{j\uparrow} + c^\dagger_{i\uparrow} c_{i\uparrow} c^\dagger_{j\uparrow} c_{j\uparrow}) \\ &= -C^\dagger_{ij} C_{ij} + \frac{1}{4} \rho_i \rho_j \end{aligned} \tag{2.34}$$

where $C^\dagger_{ij} = 1/\sqrt{2}(c^\dagger_{i\uparrow} c^\dagger_{j\downarrow} - c^\dagger_{i\downarrow} c^\dagger_{j\uparrow})$ is the "pair creation" operator, and $\rho_i = (c^\dagger_{i\uparrow} c_{i\uparrow} + c^\dagger_{i\downarrow} c_{i\downarrow})$ is electron density operator.

Finally the reduced t-J Hamiltonian has the form

$$H = H_0 + H_{pair}, \tag{2.35}$$

where

$$H_{pair} = -\frac{J}{2} \sum_{\mathbf{ij}} (c^\dagger_{i\uparrow} c^\dagger_{j\downarrow} - c^\dagger_{i\downarrow} c^\dagger_{j\uparrow})(c_{j\downarrow} c_{i\uparrow} - c_{j\uparrow} c_{i\downarrow}). \tag{2.36}$$

In case when $J_x = J_y \neq J_z$, (which is the general case for a system with the tetragonal symmetry), we have

$$\begin{aligned} J_z S^z_i S^z_j + J(S^x_i S^x_j + S^y_i S^y_j) &= \frac{J}{2} c^\dagger_{i\uparrow} c^\dagger_{j\downarrow} c_{j\uparrow} c_{i\downarrow} + \frac{J}{2} c^\dagger_{i\downarrow} c^\dagger_{j\uparrow} c_{j\downarrow} c_{i\uparrow} \\ -\frac{J_z}{2} c^\dagger_{i\uparrow} c^\dagger_{j\downarrow} c_{j\downarrow} c_{i\uparrow} - \frac{J_z}{2} c^\dagger_{i\downarrow} c^\dagger_{j\uparrow} c_{j\uparrow} c_{i\downarrow} + \frac{J_z}{4} \rho_i \rho_j. \end{aligned} \tag{2.37}$$

The last two terms in (2.37) represent the pairing interaction

$$H_{pair} = -\frac{J}{2} c^\dagger_{i\uparrow} c^\dagger_{j\downarrow} c_{i\downarrow} c_{j\uparrow} - \frac{J}{2} c^\dagger_{j\uparrow} c^\dagger_{i\downarrow} c_{j\downarrow} c_{i\uparrow} - \frac{J_z}{2} c^\dagger_{i\uparrow} c^\dagger_{j\downarrow} c_{j\downarrow} c_{i\uparrow} - \frac{J_z}{2} c^\dagger_{j\uparrow} c^\dagger_{i\downarrow} c_{i\downarrow} c_{j\uparrow}. \tag{2.38}$$

The momentum representation of H_{pair}, by using

$$c_{i\sigma} = \frac{1}{\sqrt{N}} \sum_{\mathbf{k} \in BZ} e^{i\mathbf{k}R_i} c_{\mathbf{k}\sigma}, \tag{2.39}$$

where $\mathbf{k}$ is in the wave vector in first Brillouin zone, is

$$H_{pair} = -\frac{1}{2}\frac{1}{N^2}\sum_{\mathbf{k_1k_2k_3k_4}} c^{\dagger}_{\mathbf{k}_1\uparrow}c^{\dagger}_{\mathbf{k}_2\downarrow}c_{\mathbf{k}_3\downarrow}c_{\mathbf{k}_4\uparrow}\sum_{\mathbf{ij}}\Big[Je^{-i\mathbf{k}_1\mathbf{R}_i-i\mathbf{k}_2\mathbf{R}_j+i\mathbf{k}_3\mathbf{R}_i+i\mathbf{k}_4\mathbf{R}_j} + Je^{-i\mathbf{k}_1\mathbf{R}_j-i\mathbf{k}_2\mathbf{R}_i+i\mathbf{k}_3\mathbf{R}_j+i\mathbf{k}_4\mathbf{R}_i}$$
$$+J_ze^{-i\mathbf{k}_1\mathbf{R}_i-i\mathbf{k}_2\mathbf{R}_j+i\mathbf{k}_3\mathbf{R}_j+i\mathbf{k}_4\mathbf{R}_i} + J_ze^{-i\mathbf{k}_1\mathbf{R}_j-i\mathbf{k}_2\mathbf{R}_i+i\mathbf{k}_3\mathbf{R}_i+i\mathbf{k}_4\mathbf{R}_j}\Big], \tag{2.40}$$

where

$$\mathbf{j} = \mathbf{i} + \mathbf{a}.$$

where $\mathbf{a}$ connects nearest neighbors. So we can rewrite the last four terms of (2.40) as

$$S_1 = NJ\sum_i e^{i(-\mathbf{k}_1-\mathbf{k}_2+\mathbf{k}_3+\mathbf{k}_4)\mathbf{R}_i}\sum_{\mathbf{a}} e^{(\mathbf{k}_4-\mathbf{k}_2)\mathbf{a}}$$
$$= NJ\delta_{\mathbf{k}_1+\mathbf{k}_2,\mathbf{k}_3+\mathbf{k}_4}\sum_{\mathbf{a}} e^{(\mathbf{k}_4-\mathbf{k}_2)\mathbf{a}}, \tag{2.41}$$

$$S_2 = NJ\sum_i e^{i(-\mathbf{k}_1-\mathbf{k}_2+\mathbf{k}_3+\mathbf{k}_4)\mathbf{R}_i\mathbf{R}_i}\sum_{\mathbf{a}} e^{(\mathbf{k}_3-\mathbf{k}_1)\mathbf{a}}$$
$$= NJ\delta_{\mathbf{k}_1+\mathbf{k}_2,\mathbf{k}_3+\mathbf{k}_4}\sum_{\mathbf{a}} e^{(\mathbf{k}_3-\mathbf{k}_1)\mathbf{a}}, \tag{2.42}$$

$$S_3 = NJ_z\delta_{\mathbf{k}_1+\mathbf{k}_2,\mathbf{k}_3+\mathbf{k}_4}\sum_{\mathbf{a}} e^{(\mathbf{k}_3-\mathbf{k}_2)\mathbf{a}}, \tag{2.43}$$

and

$$S_4 = NJ_z\delta_{\mathbf{k}_1+\mathbf{k}_2,\mathbf{k}_3+\mathbf{k}_4}\sum_{\mathbf{a}} e^{(\mathbf{k}_4-\mathbf{k}_1)\mathbf{a}}. \tag{2.44}$$

If we introduce $\mathbf{k_1} + \mathbf{k_2} = \mathbf{q} = \mathbf{k_3} + \mathbf{k_4}$, (2.40) can be rewritten as

$$H_{pair} = \frac{1}{N}\sum_{\mathbf{k},\mathbf{k'q}} V_d(\mathbf{k},\mathbf{k'})\, c^{\dagger}_{\mathbf{k}+\frac{\mathbf{q}}{2},\uparrow}c^{\dagger}_{-\mathbf{k}+\frac{\mathbf{q}}{2},\downarrow}c_{-\mathbf{k'}+\frac{\mathbf{q}}{2},\downarrow}c_{\mathbf{k'},\uparrow}$$
$$+ \frac{1}{N}\sum_{\mathbf{k},\mathbf{k'q}} V_s(\mathbf{k},\mathbf{k'})\, c^{\dagger}_{\mathbf{k}+\frac{\mathbf{q}}{2},\uparrow}c^{\dagger}_{-\mathbf{k}+\frac{\mathbf{q}}{2},\downarrow}c_{-\mathbf{k'}+\frac{\mathbf{q}}{2},\downarrow}c_{\mathbf{k'},\uparrow}$$
$$+ \frac{1}{N}\sum_{\mathbf{k},\mathbf{k'q}} V_p(\mathbf{k},\mathbf{k'})\, c^{\dagger}_{\mathbf{k}+\frac{\mathbf{q}}{2},\uparrow}c^{\dagger}_{-\mathbf{k}+\frac{\mathbf{q}}{2},\downarrow}c_{-\mathbf{k'}+\frac{\mathbf{q}}{2},\downarrow}c_{\mathbf{k'},\uparrow}, \tag{2.45}$$

where

$$V_d = -(J + J_z)\phi_d(\mathbf{k})\phi_d(\mathbf{k'}),$$
$$V_s = -(J + J_z)\phi_s(\mathbf{k})\phi_s(\mathbf{k'}), \tag{2.46}$$

and

$$V_p = -2(J - J_z)[\phi_p^{(1)}(\mathbf{k})\phi_p^{(1)}(\mathbf{k}') + \phi_p^{(2)}(\mathbf{k})\phi_p^{(2)}(\mathbf{k}')], \tag{2.47}$$

where for singlet case we can define basis functions, $\phi_s(\mathbf{k})$, and $\phi_d(\mathbf{k})$, for the extended s-wave and d-wave ($d_{x^2-y^2}$) pairings as

$$\phi_d(\mathbf{k}) = \cos k_x a - \cos k_y a, \tag{2.48}$$

and

$$\phi_s(\mathbf{k}) = \cos k_x a + \cos k_y a. \tag{2.49}$$

For the triplet case we introduce $\phi_p(\mathbf{k})$, the basis function for p-wave pairing, as

$$\phi_p^{(1)}(\mathbf{k}) = \sin k_x a \quad , \quad \phi_p^{(2)}(\mathbf{k}) = \sin k_y a. \tag{2.50}$$

The pairing interactions in the d-wave and the extended s-wave channels are the same, while the p-wave channel splits from s and d. The symmetry of the orbital part of the wave function is even for s-wave and d-wave pairings while it is odd for p-wave pairing. Since the total wave function of the pair is a product of the orbital part of the wave function and the spin part of the wave function, it follows that the spin part of the wave function should change sign when the two electrons are interchanged for s-wave and d-wave pairing. For p-wave pairing on the other hand, the spin part should remain unchanged. The coupling in the s-wave channel is expected to be suppressed because of a strong on-site Coulomb repulsion between the electrons. In this thesis, we are considering the d-wave pairing.

2.7.2 Bogoliubov-de Gennes equations

In section 2.5 we discussed the microscopic BSC theory which is valid only for pure materials, in which the wave vector $\mathbf{k}$ is a good quantum number, and the $\mathbf{k}\uparrow$ and $-\mathbf{k}\downarrow$ states are occupied in pairs. When there are spatial variations in the Hamiltonian, such as, an external vector-potential $\mathbf{A}(\mathbf{r})$, or scattering centers described by the potential $U(\mathbf{r})$, or a variation in $\Delta(\mathbf{r})$ imposed by vortex core, the plane-wave momentum eigenfunctions characterized by $\mathbf{k}$ used in original BSC development are no longer appropriate. They should be replaced by suitable position-dependent function [7].

Consider a homogeneous electron gas in a magnetic field $\mathbf{B} = \nabla \times \mathbf{A}$. The Hamiltonian is given by

$$H = \int d\mathbf{r} \sum_{\sigma} \Psi^{\dagger}(\mathbf{r}\sigma) H_e \Psi(\mathbf{r}\sigma) - \frac{1}{2} V \int d\mathbf{r} \sum_{\sigma\sigma'} \Psi^{\dagger}(\mathbf{r}\sigma)\Psi^{\dagger}(\mathbf{r}\sigma')\Psi(\mathbf{r}\sigma)\Psi(\mathbf{r}\sigma'), \tag{2.51}$$

where

$$H_e(\mathbf{r}) = \frac{1}{2m}\left(-i\hbar\nabla - \frac{e\mathbf{A}}{c}\right)^2 + U(\mathbf{r}) - E_F,$$

and $\Psi(\mathbf{r}\sigma)$ is the field operator. If in (2.51), we replace the interaction $V\Psi^{\dagger}\Psi^{\dagger}\Psi\Psi$ by an average potential acting on only one particle at a time (therefore only containing two operators Ψ and $\Psi^{\dagger}$), we may get the effective Hamiltonian of the form

$$H_{eff} = \int d\mathbf{r}\{\sum_{\sigma} \Psi^{\dagger}(\mathbf{r}\sigma) H_e \Psi(\mathbf{r}\sigma) + U(\mathbf{r})\Psi^{\dagger}(\mathbf{r}\sigma)\Psi(\mathbf{r}\sigma) + \Delta(\mathbf{r})\Psi^{\dagger}(\mathbf{r}\uparrow)\Psi^{\dagger}(\mathbf{r}\downarrow) + \Delta^{*}(\mathbf{r})\Psi(\mathbf{r}\downarrow)\Psi(\mathbf{r}\uparrow)\}. \tag{2.52}$$

We suppose H_{eff} is known. In order to find the eigenstates and corresponding energies, we perform a unitary transformation

$$\begin{aligned} \Psi(\mathbf{r}\uparrow) &= \sum_{n} (\gamma_{n\uparrow} u_n(\mathbf{r}) - \gamma^{\dagger}_{n\downarrow} v^{*}_n(\mathbf{r})), \\ \Psi(\mathbf{r}\downarrow) &= \sum_{n} (\gamma_{n\downarrow} u_n(\mathbf{r}) - \gamma^{\dagger}_{n\uparrow} v^{*}_n(\mathbf{r})), \end{aligned} \tag{2.53}$$

where γ and $\gamma^{\dagger}$ are quasiparticle operators satisfying the fermion commutation relations and n is the number of states below the Fermi level

$$\begin{aligned} \{\gamma_{n\sigma}, \gamma^{\dagger}_{m\sigma'}\} &= \delta_{mn}\delta_{\sigma\sigma'}, \\ \{\gamma_{n\sigma}, \gamma_{m\sigma'}\} &= 0, \end{aligned} \tag{2.54}$$

by using (2.53), the effective Hamiltonian, H_{eff}, must be diagonalized as

$$H_{eff} = E_g + \sum_{n,\sigma} \epsilon_n \gamma^{\dagger}_{n\sigma}\gamma_{n\sigma} \tag{2.55}$$

where E_g is the groundstate energy of H_{eff} and ϵ_n is the energy of excitation n. By using (2.51) and (2.53), we can calculate the anticommution properties of Ψ and H_{eff} and obtain the well-known Bogoliubov-de Gennes (BdG) equations:

$$\begin{aligned} [H_e + U(\mathbf{r})]u(\mathbf{r}) + \Delta(\mathbf{r})v(\mathbf{r}) &= \epsilon u(\mathbf{r}), \\ -[H^{*}_e + U(\mathbf{r})]v(\mathbf{r}) + \Delta^{*}(\mathbf{r})u(\mathbf{r}) &= \epsilon v(\mathbf{r}). \end{aligned} \tag{2.56}$$

These equations can be written compactly in a matrix form

$$\begin{pmatrix} H_e + U & \Delta(\mathbf{r}) \\ \Delta^*(\mathbf{r}) & -H_e^* - U \end{pmatrix} \begin{pmatrix} u \\ v \end{pmatrix} = \epsilon \begin{pmatrix} u \\ v \end{pmatrix}, \tag{2.57}$$

where

$$\Delta(\mathbf{r}) = V \sum_n v_n^*(\mathbf{r}) u_n(\mathbf{r})(1 - 2f_n),$$

and

$$f_n = \frac{1}{\exp(\beta\epsilon_n) + 1}.$$

is the Fermi function. The derivation above is valid for an s-wave superconductor. The situation in a d-wave superconductor is different from the classic s-wave case: when the pairing state has a finite angular momentum and is not a global eigenstate of the angular momentum L_z (a d-wave superconductor is an equal admixture of $L_z = \pm 1$ states), the problem can not be reduced to a collection of decoupled 1D eigenvalue equations for each angular momentum channel. Instead all channels remain coupled and must be solved as a full 2D problem.

The natural starting point of the calculating BdG Hamiltonian in a d-wave superconductor, is the mean-field BCS Hamiltonian written in the second quantization form[7],

$$\begin{aligned} H = &\int d\mathbf{x} \psi_\sigma^\dagger(\mathbf{x}) \left[\frac{1}{4m} \left(\mathbf{p} - \frac{e}{c} \mathbf{A} \right)^2 - \mu \right] \psi_\sigma(\mathbf{x}) \\ &+ \int d\mathbf{x} \int d\mathbf{y} \left[\Delta(\mathbf{x}, \mathbf{y}) \psi_\uparrow^\dagger(\mathbf{x}) \psi_\downarrow^\dagger(\mathbf{y}) + \Delta^*(\mathbf{x}, \mathbf{y}) \psi_\uparrow(\mathbf{y}) \psi_\downarrow(\mathbf{x}) \right], \end{aligned} \tag{2.58}$$

where $\Delta(\mathbf{x}, \mathbf{y})$ is the pairing field. We define an integral operator $\hat{\Delta}$ such that [8]:

$$\hat{\Delta} \psi(\mathbf{x}) = \int d\mathbf{y} \Delta(\mathbf{x}, \mathbf{y}) \psi(\mathbf{y}). \tag{2.59}$$

On a tight-binding lattice the vortex flux is concentrated inside the plaquette and thus the length-scale associated with the core is implicitly the lattice spacing a of the underlying tight-binding lattice [9]. The d-wave pairing operator in the vortex state can be written as a differential operator:

$$\hat{\Delta} = \Delta_0 \sum_{\mathbf{a}} \eta_a \exp\left[i \frac{\phi(\mathbf{x})}{2} \right] \exp(i\mathbf{a} \cdot \mathbf{p}) \exp\left[i \frac{\phi(\mathbf{x})}{2} \right], \tag{2.60}$$

the sums are over nearest neighbors and on the square tight-binding lattice $a = \pm\hat{x}, \pm\hat{y}$, the operator η_a

$$\eta_a = \begin{cases} 1 & \text{along x axis,} \\ -1 & \text{along y axis,} \end{cases} \tag{2.61}$$

follows from the d-wave pairing: $\Delta = 2\Delta_0(\cos k_x a - \cos k_y a)$. The Hamiltonian (2.58) can be written in Nambu formalism as

$$H = \int d\mathbf{x}\Psi^\dagger \hat{H}_0 \Psi(\mathbf{x}), \tag{2.62}$$

where the Nambu spinor $\Psi^\dagger = (\psi_\uparrow^\dagger, \psi_\downarrow)$, and the matrix differential operator is

$$\hat{H}_0 = \begin{pmatrix} \hat{h} & \hat{\Delta} \\ \hat{\Delta}^* & -h^* \end{pmatrix}, \tag{2.63}$$

where in the tight-binding lattice:

$$\hat{h} = -t \sum_{\mathbf{a}} \exp\left[i \int_{\mathbf{x}}^{\mathbf{x}+\mathbf{a}} \left(\mathbf{p} - \frac{e}{c}\mathbf{A} \right) \cdot d\mathbf{r} \right] - \mu. \tag{2.64}$$

This leads to BdG equations

$$\hat{H}_0 \Phi_n = \epsilon_n \Phi_n. \tag{2.65}$$

The solutions of these coupled differential equations are quasiparticle wave functions that are rank two spinors in the Nambu space, $\Phi^T(\mathbf{r}) = (u(\mathbf{r}), v(\mathbf{r}))$. Using BdG equations we can study impurity effects and vortex properties in a d-wave superconductor.

2.8 Impurities

The role of impurities in superconductors has been studied theoretically since the establishment of BCS theory. The main reason is that the superconducting properties are qualitatively modified by impurity atoms. In principle, these observations can be useful as a method of identifying the nature of the pairing state in superconductors. In conventional (s-wave) superconductors, the statement that non-magnetic impurities affect neither the transition temperature nor the superfluid density is known as Anderson's theorem [10]. On the other hand, impurities have strong effects on the superconducting properties of unconventional superconductors.

In the case of the high T_c superconductors, a large number of experimental results and theories support the d-wave pairing state. The significant difference between d-wave pairing state and the conventional one is that, in the d-wave state, the order parameter (pair potential) changes its sign with $\pi/2$ rotation. Thus the nodes of energy gap exist on the fermi surface along the $k_x = \pm k_y$

directions in Brillouin zone. Being intrinsically anisotropic, d-wave superconductors are strongly affected even by non-magnetic impurities. Because of the energy gap anisotropy strong impurities can cause a strong pair-breaking effect. The Zn substitutions in cuprates are one example of this. Although Zn atoms are normally non-magnetic, T_c is strongly suppressed by Zn substitution of Cu in the planes. Therefore it is reasonable to assume that Zn ions behave as non-magnetic unitary scatterers. A strongly scattering scalar impurity is a requirement for a localized bound state to exist in a d-wave superconductor. Indeed, the low-lying quasiparticle states close to the nodes in the energy gap will be strongly influenced even by non-magnetic impurity potential [11]. In this thesis, we consider a point-like impurity, Zn atom, in our model. Experimentally, the effect of a single strong impurity on the electronic properties of superconductors can be studied using the scanning tunneling microscopy technique.

Chapter 3

Review of STM experimental data

In this Chapter we give a brief view of the relevant experimental results. Since it is known that the superconductivity occurs in the copper-oxide layer, scanning tunneling microscopy (STM) experiments were used to probe low energy states associated with the vortex cores in BSCCO. We focus on the experimental observations on the BSCCO crystals where a very small fraction of their copper atoms replaced by Zn atoms, in an applied magnetic field perpendicular to the surface. The low energy spectra at the impurities and vortices are sufficiently distinct from each other that the scattering resonances and the vortex cores can be independently imaged. This can be done by taking simultaneous DOS maps at zero bias and the core state energy, respectively [12].

3.1 Scanning tunneling microscopy

3.1.1 The basics of scanning tunneling microscopy

The scanning tunneling microscope was invented in 1982 by Binnig and Rohrer [13], for which they shared the 1986 Nobel Prize in Physics. The instrument consists of a sharp conducting tip which is scanned with respect to a flat conducting sample. When a voltage V is applied between tip and sample, a current will flow, and this current can be measured as a function of (x,y) location and as a function of V. This is illustrated schematically in Fig. 3.1.

The tip is just a very sharp needle, so sharp that it terminates in a single atom. It is not actually touching the sample, rather it is approximately a few atomic diameters away. The tip is held at zero voltage. Meanwhile, a bias voltage is placed on the sample, on the order of a few millivolts to a few volts. This voltage bias induces a tunneling current to flow between the tip and the sample. This current is exponentially dependent upon the distance between the tip and the sample which

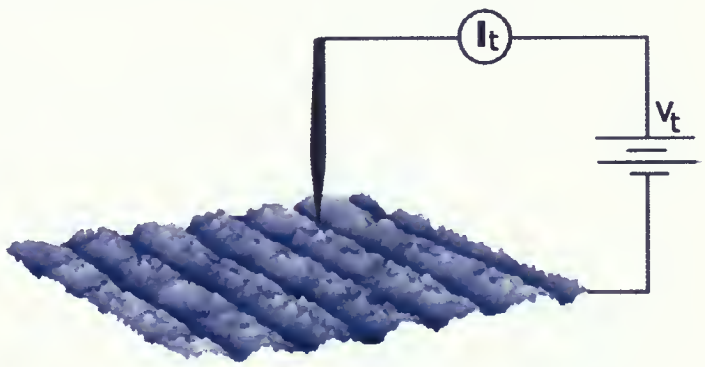

Figure 3.1: Schematic of STM tip and sample. A bias voltage V is applied to the sample, the tunneling current I is measured as V and/or the (x, y) position of the tip are varied.

means that for a small change in the distance between the tip and the sample the current changes by alot.

The tip can be scanned across the surface using a piezoelectric crystal, which changes its size by very small amounts when a voltage is applied to it. As the tip is moved in the x or y direction along the surface of the sample, the current will vary according to whether the tip is right on top of an atom (smaller distance), or on top of a space between atoms (larger distance). So an individual atom can be "seen" as an increase in the tunneling current as the xy scan control moves the tip across the surface of the sample.

In practice, since current falls off exponentially with distance, the current when the tip is on top of an atom is much much larger than the current when the tip is between atoms. We could just record the current as a function xy position on the surface, but because the current is exponential in the tip-sample distance this would give a distorted image in which the atomic peaks would look much higher than they actually are.

3.1.2 Calculation of tunneling current

The current which flows between the tip and the sample can be calculated by time dependent perturbation theory [14]. If the sample is biased by a negative voltage -V with respect to the tip, this effectively raises the Fermi level of the sample electrons with respect to the tip electrons.

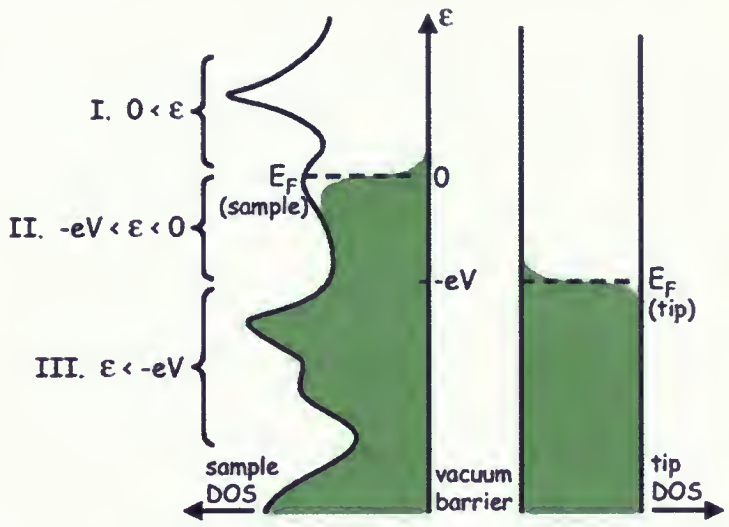

Figure 3.2: Schematic of tip-sample tunneling. Energy is along the vertical axis, and density of states of the sample and tip are shown along the horizontal axes. Filled states are shown in grey. In this case, a negative bias voltage -V has been applied to the sample, which effectively raises its Fermi level by eV with respect to the Fermi level of the tip. This allows for filled states on the left (sample) to tunnel into empty states on the right (tip).

Electrons will tend to flow out of the filled states of the sample, into the empty states of the tip. This situation is illustrated in Fig. 3.2. The elastic tunneling current from the sample to the tip for states of energy ϵ (with respect to the Fermi level of the sample) is:

$$I_{sample \rightarrow tip} = -2e\frac{2\pi}{\hbar}|M|^2\{\rho_s(\epsilon)f(\epsilon)\}\{\rho_t(\epsilon + eV)[1 - f(\epsilon + eV)]\}, \tag{3.1}$$

where the first brackets shows the number of filled sample states for tunneling from and the second one shows the number of empty sample states for tunneling to. The factor of 2 out front is for spin, -e is the electron charge (we are tunneling single electrons, not Cooper pairs), $2\pi/\hbar$ comes from time-dependent perturbation theory, $|M|^2$ is the matrix element, $\rho_{s(t)}(\epsilon)$ is the density of states of the sample (tip), and $f(\epsilon)$ is the Fermi distribution. Though the dominant tunneling current for negative sample voltage -V will be from sample to tip, there will also be a smaller tunneling current of electrons from tip to sample:

$$I_{tip \to sample} = -2e\frac{2\pi}{\hbar}|M|^2\{\rho_t(\epsilon + eV)f(\epsilon + eV)\}\{\rho_s(\epsilon)[1 - f(\epsilon)]\}. \tag{3.2}$$

When we sum these, and integrate over all energies ϵ, we arrive at the total tunneling current from sample to tip:

$$I = -\frac{4\pi e}{\hbar}\int_{-\epsilon_F(tip)}^{\infty}|M|^2\rho_s(\epsilon)\rho_t(\epsilon + eV)\{f(\epsilon)[1 - f(\epsilon + eV)] - [1 - f(\epsilon)]f(\epsilon + eV)\}d\epsilon. \tag{3.3}$$

The relevant range of ϵ over which we must integrate to find the tunneling current is reduced to $-eV < \epsilon < 0$. (Likewise, if we had applied a positive bias voltage V to the sample, our range of integration would be $0 < \epsilon < eV$.) So we are left with approximately:

$$I = -\frac{4\pi e}{\hbar}\int_{-eV}^{0}|M|^2\rho_s(\epsilon)\rho_t(\epsilon + eV)d\epsilon. \tag{3.4}$$

Experimentalists pick a tip material which has a flat density of states within the energy range of the Fermi surface that they wish to study so that $\rho_t(\epsilon + eV)$ in (3.4) can be treated as a constant and taken outside the integral. We can write (3.4) as

$$I = I_0\int_{-eV}^{0}\rho_s(\epsilon)d\epsilon. \tag{3.5}$$

In other words, we can measure the integral of the density of states down to any energy $-eV$ by varing V.

3.1.3 Scanning tunneling microscope measurements

An STM can typically measure and control the current that flows between the tip and the sample (I), the bias voltage between the tip and the sample (V), the xy (in sample plane) position of the tip, and the z (perpendicular to sample plane) distance between the tip and sample. The STM visualizes a three dimensional density of states (DOS) for each x and y position of energy and measures the quantity local density of states (LDOS) as a function of position on the surface (controlled by where the tip is above the surface) and as a function of energy (controlled by the bias voltage between the tip and sample). The LDOS is the density of the electrons of certain energy at particular special location. The LDOS is proportional to the differential increase in tunneling current given

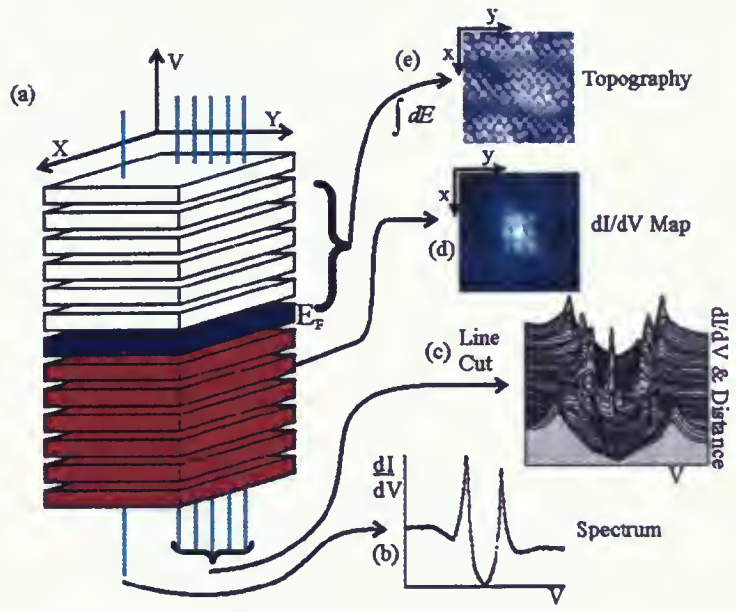

Figure 3.3: (a) Since an STM can measure dI/dV(x,y,V), this figure schematically represents the x,y and V values at which an STM can measure the conductance. Each plane represents a different value of the tip-sample bias V, and the lateral position on the plane gives the x,y position of the tip. Filled states are given in grey. The plane at the Fermi energy (V=0) is shown in blue. Panels (b) - (e) show subsets of this full data-set. The relation of the subset to the full data-set is shown schematically, and the name of each subset and a typical example of each from BSCCO is shown.

a differential increase in bias voltage or in other words one can measure the LDOS by measuring dI/dV. We call this dI/dV the conductance $g(V)$,

$$g(V) \equiv \frac{dI}{dV} \propto DOS(eV). \tag{3.6}$$

Therefore, by varying V , we can map out an entire density of states curve.

A dI/dV Map shows the density of electrons at a particular energy as a function of position on the surface. In Fig. 3.3, a dI/dV map is equivalent to view a single energy plane. Impurity atoms on the surface attract electrons of a certain energy so at that energy they are bright in the dI/dV maps. In Fig. 3.3, the position of an impurity atom is indicated by the center of the clover leaf pattern in the blue dI/dV map. However, in general at a random energy there will be no especially high

electron density at any given position, but rather the electron density will be uniform throughout the surface of the crystal. This means that the dI/dV map will be uniformly black as indicated by the black panel in Fig. 3.3.

A superconductor has a very low density of states at low energies. The spectrum shown in Fig. 3.3 is the spectrum for a d-wave superconductor and we can see that the density of states decreases as we move to lower energies (zero energy is in the middle of the graph). BSCCO is a d -wave superconductor; the bound electrons in the Cooper pairs have d -wave, four-fold symmetry. This means that the energy landscape is directions. In BSCCO, an electron entering the tip from one direction may see a 10 meV square gap, while an electron entering from another direction may see a 30 meV square gap. What measures with an STM is a sum of all these processes from every direction. The average of all the square gaps gives us a V-shaped gap. Therefore, each individual STM spectrum forfeits the **k**-space information. In Fig. 3.4 we compare the density of states and $\Delta(\mathbf{k})$ for a d-wave and a s-wave superconductor.

3.1.4 Low-T_c and cuprate vortex phenomenology

Scanning tunneling microscopy can be used to image the additional quasiparticle states generated by quantized vortices in BSCCO. In an ideal metal, the Landau quasiparticle eigenstates are Bloch wavefunctions characterized by wavevector **k**. The LDOS spectrum at a single location **r** is related to the **k**-space eigenstates $\Psi_{\mathbf{k}}(\mathbf{r})$ by

$$LDOS(E, \mathbf{r}) \propto \sum_{\mathbf{k}} |\Psi_{\mathbf{k}}(\mathbf{r})|^2 \delta(E - \epsilon(\mathbf{k})). \tag{3.7}$$

Since LDOS is proportional to the norm of the quasiparticle wavefunction $|\Psi_k|^2$, the LDOS will contain an interference pattern with wavevector $\mathbf{q} = \mathbf{k}_1 - \mathbf{k}_2$, or wavelength $\lambda = 2\pi/q$. LDOS modulations can be observed by STM as spatial modulations of the differential tunneling conductance dI/dV.

The Bogoliubov quasiparticles in a uniform BCS superconductor are described by the Bloch wavefunctions, but with dispersion

$$E(\mathbf{k}) = \sqrt{\epsilon^2(\mathbf{k}) + \Delta^2(\mathbf{k})}, \tag{3.8}$$

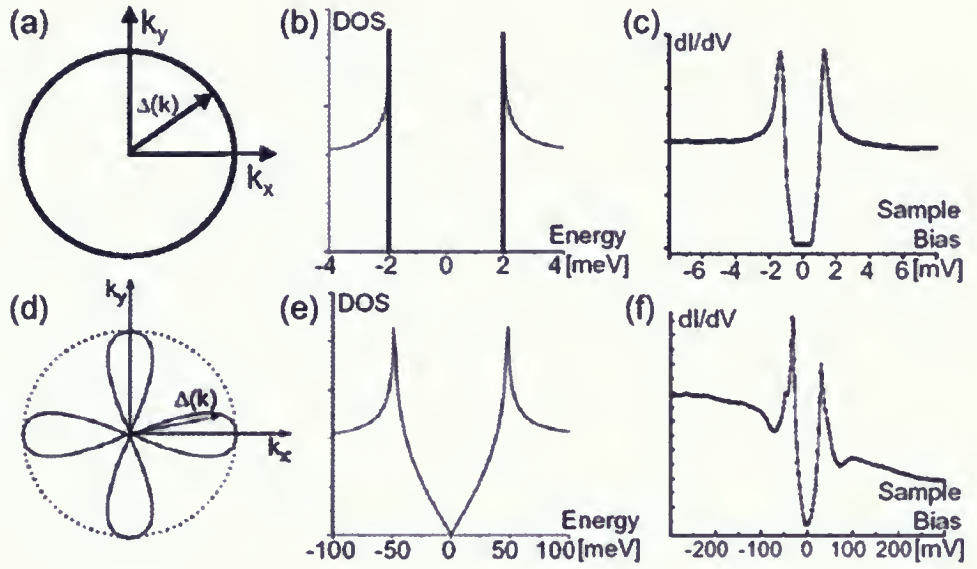

Figure 3.4: Demonstration of the density of states, as seen by an STM, averaged over $\mathbf{k}$ for s-wave and d-wave superconductors. (a) Gap $\Delta(\mathbf{k})$ is constant as a function of angle for an s-wave superconductor. (b) Therefore when the STM averages over angle, the resultant density of states still shows a square gap. (c) Real data:[15] density of states spectrum on s-wave superconductor $NbSe_2$. The imperfection of the square gap is due in part to thermal broadening, and in part to the very slight anisotropy in the $NbSe_2$ s-wave gap. (d) Gap $\Delta(\mathbf{k})$ is angle-dependent for a d-wave superconductor. (e) Therefore, when the STM averages over angle, it combines square-gapped spectra with all different values of Δ, and the resultant average shows a V-shaped gap. (f) Real data: typical density of states spectrum on d-wave superconductor BSCCO.

where $|\Delta(\mathbf{k})|$ is the $\mathbf{k}$-dependent magnitude of the energy gap at the Fermi surface.

To find the superconducting state band structure, we need a formula for the superconducting gap as a function of angle, $\Delta_{\mathbf{k}}$. Several possibilities exist in the literature. One of the most popular choices is [16]:

$$\Delta_{\mathbf{k}} = 2\Delta_0[\cos k_x a - \cos k_y a]. \tag{3.9}$$

In conventional s-wave type-II superconductors, the superconducting order parameter is suppressed in the cores of quantized magnetic vortices, and recovers over a distance of about one coherence length ξ, as discussed in Sec. 2.3. Bound quasiparticle states can exist inside these cores [17] with lowest energy given approximately by $E \sim \Delta^2/2\epsilon_F$, where ϵ_F is the Fermi energy and Δ is the superconducting gap. Such "core" states at the Fermi energy were first imaged by Hess et al. using low temperature STM [18].

A simple description of a vortex in an s-wave superconductor is a particle-in-a-box. In the vortex core, the superconducting order parameter is destroyed, so the quasiparticle has no binding energy and can exist freely. However, outside the vortex "box", the unattached quasiparticle has energy Δ greater than it would have if joined into a Cooper pair. So we can think of the quasiparticle as sitting in a circular potential well of height Δ and radius ξ. No matter how shallow the well, there will exist at least one bound state, which will decay exponentially outside the box [19].

However, the cuprate superconductors have a $d_{x^2-y^2}$ order parameter. This means there are four gap nodes, which would imply that there are four holes in the walls of the vortex "box". So we might expect that such a "leaky" box would contain only scattering states, which decay as a power law with distance. Indeed, initial theoretical efforts focused on the quantized vortex in an otherwise conventional BCS superconductor with $d_{x^2-y^2}$ symmetry [20]-[23]. These models included predictions that, because of the gap nodes, the local density of electronic states (LDOS) inside the core is strongly peaked at the Fermi level. This peak, which would appear in tunneling studies as a zero bias conductance peak (ZBCP), should display a four-fold symmetric star shape oriented toward the gap nodes, and decaying as a power law with distance. Scanning tunneling microscopy studies of HTSC vortices have revealed a very different electronic structure from that predicted by the pure d-wave BCS models. Vortices in $YBa_2Cu_3O_{7\delta}$ (YBCO) lack ZBCPs but exhibit additional

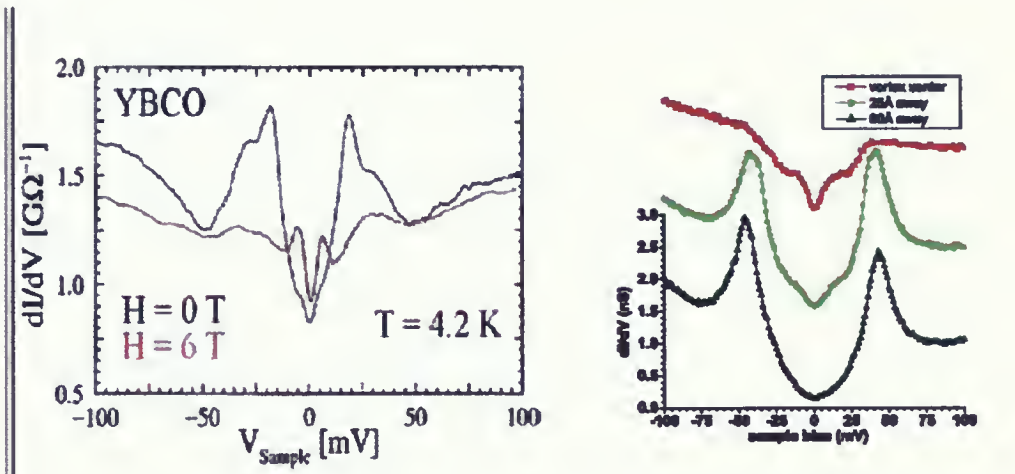

(a) $YBa_2Cu_3O_{7-\delta}$ (b) $Bi_2Sr_2CaCu_2O_{8+\delta}$

Figure 3.5: Density of states spectra from (a)$YBa_2Cu_3O_{7-\delta}$ (from Maggio-Aprile *et* al. [26]) and (b)$Bi_2Sr_2CaCu_2O_{8+\delta}$ (adapted from Pan *et* al. [25]) Red traces show spectra inside the vortex cores, while black traces show spectra taken far from the vortices. In (b) it also shows a spectrum at an intermediate distance (green trace), outside the vortex "core" but still clearly influenced by the vortex.

quasiparticle states at 5.5 meV [24], whereas those in BSCCO also lack ZBCPs [25]. More recently, the additional quasiparticle states at BSCCO vortices were discovered at energies near 7 meV [12]. Typical DOS spectra from BSCCO and YBCO vortex cores are shown in Fig. 3.5.

Thus, a common phenomenology for low energy quasiparticles associated with vortices is becoming apparent. Its features include:

1. The absence of ZBCP's.
2. Low energy quasiparticle states at ±5.5 meV (YBCO) and ±7 meV (Bi-2212).
3. A radius for the actual vortex core (where the coherence peaks are absent) of ∼10 Å, [12].
4. A radius of up to 75 Å, within which these states are detected, and apparently decay exponentially [12].
5. The absence of a four-fold symmetric star-shaped LDOS.

3.2 Interaction between impurities and vortices

In order to better understand the electronic properties of the high temperature superconductor $Bi_2Sr_2CaCu_2O_{8+\delta}$, experimentalists from the Berkeley group studied samples in which some of the Cu atoms in the superconducting CuO_2 plane have been intentionally replaced by impurity atoms. The particular impurity atoms used have distinct magnetic and electrostatic properties which perturb the superconductor to produce a characteristic pattern in the local density of states. This pattern is then imaged by scanning tunnelling microscopy and spectroscopy in order to produce atomic scale information about the local effects of these perturbations. In general, there are quasiparticle resonances within the superconducting energy gap whose spatial extent are clearly fourfold in keeping with the d-wave gap symmetry. The experimentalists are looking in the case when Cu is replaced by a single point like strong impurity like Zn. Zn is a supposed non-magnetic impurity known to replace copper in the superconducting CuO_2 plane of BSCCO. STM and other probes indicate that it is destructive to superconductivity.

Fig. 3.6(b) is measured at $V = 7\ mV$ in a magnetic field of 7.25 T on identical area as Fig. 3.6(a) and contains regions of enhanced DOS with apparent radius near 60 Å, associated with vortices [12]. The ability of mapping vortex and impurity locations independently, allows one to study interaction between them. The STM experiments [12] shows that the Zn impurity atoms provide attractive potentials for pinning of the vortices and their random distribution is a source of disorder in the vortex solid.

Zooming in on an individual Zn atom with dI/dV map taken at the resonance energy, a rich spatial pattern is evident (Fig. 3.7). The central atom is the Zn atom. In addition, there is a very evident cross formed by the four second nearest neighbor atoms along the horizontal (a axis) and vertical (b axis) directions. This cross lies along the gap node directions as is expected by theory and its fourfold symmetry provides direct real space evidence of the fourfold d-wave symmetry of the energy gap in the high temperature superconductors.

If the STM tip is put directly over the center of one of the crosses we may acquire a spectrum Fig. 3.7 for the Zn atom. Compared to the usual d-wave superconductor spectrum, there is a very large peak in the Zn atom spectra at the resonance energy. Zn impurities have a peak in the density

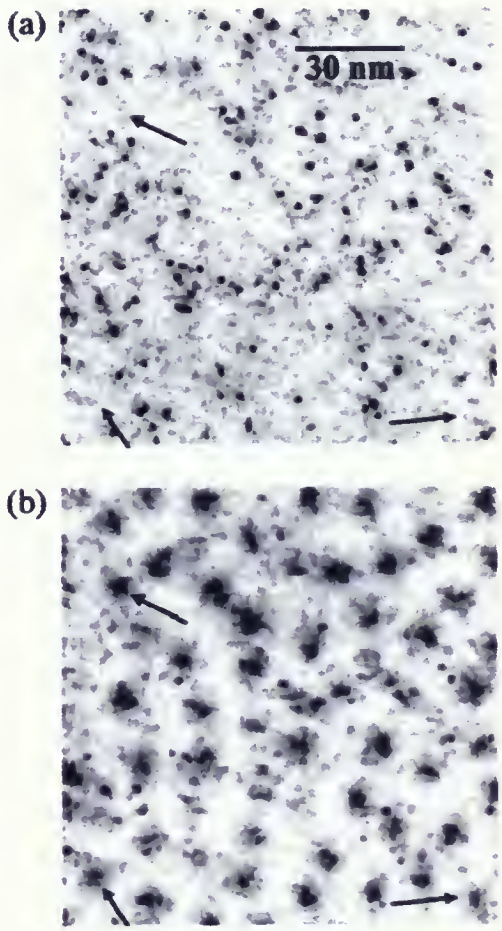

Figure 3.6: (a) A DOS map of a 120 nm square field of view, measured at zero sample bias in zero magnetic field, shows the impurity scattering resonances. (b) A DOS map, measured on the same 120 nm square field of view as (a) at sample bias V = 7 mV in B = 7.25 T shows about 50 regions of increased DOS associated with vortices. The apparent shape of the vortices varies from vortex to vortex, probably due to the influence of impurities and other inhomogeneities in the crystal. The vortex solid appears highly disordered. Comparison with (a) shows that vortices are often found at the sites of impurities, which appear to act as pin sites. Arrows indicate the locations of vortices remote from any scattering resonance.

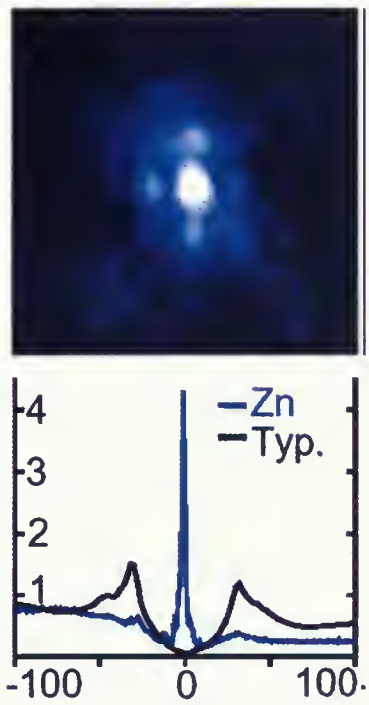

Figure 3.7: Density of states maps and spectra at Zn, in BSCCO. The spectrum at a Zn impurity shows a peak at -1.5 meV. Black curve shows typical spectra far from the impurity, for comparison. The map was measured near the peak energy of the -1.5 meV.

of states at -1.5 meV. This peak is strongest on the central atom, and falls off to about 1/5 of the value on the next nearest neighboring atoms [27].

The low energy spectra at the impurities and vortices are sufficiently distinct from each other that the scattering resonances at the vortex cores can be independently imaged. The ability to independently map vortex and impurity locations allows us to study interactions between them. In regions of high impurity density , the density of vortices are also high [12]. This can clearly be seen in the Zn doped crystals which have stronger scattering impurities. The Zn impurity atoms provide attractive potential for pinning of the vortices and their random distribution is a source for the disorder for the vortex solid.

Chapter 4

Our model

The experimental results reviewed in the preveous Chapter show that the Abrikosov vortices are attracted to strong impurities such as Zn. In this Chapter we present the computation procedure for calculating the interaction between vortices and impurities in a d-wave superconductor by a direct numerical diagonalization of the lattice Bogoliubov-De Gennes Hamiltonian. First we start with introducing all elements of our two-dimensional model in the real space. Then we explain the procedures of finding the Hamiltonian matrix for the model. Finally, we diagonalize the matrix and find the condensation energies of the system for different locations of the impurity.

4.1 The model in real space

Let us consider a two dimensional d-wave superconductor. The model consists of a tight-binding lattice with the nearest-neighbor and the next nearest-neighbor hopping, a single point-like-impurity and a single vortex on the center of the lattice. We describe our system based on the BdG Hamiltonian described in Chapter 2. The BdG Hamiltonian can be written as

$$H = -\sum_{i,\sigma} \mu c^{\dagger}_{i\sigma} c_{i\sigma} - t \sum_{<i,j>,\sigma} e^{i\phi_{ij}} c^{\dagger}_{i\sigma} c_{j\sigma} - t' \sum_{<<i,j>>,\sigma} e^{i\phi_{ij}} c^{\dagger}_{i\sigma} c_{j\sigma} + \sum_{<ij>} \left(\Delta_{ij} c^{\dagger}_{i\uparrow} c^{\dagger}_{j\downarrow} + \Delta^{\dagger}_{ij} c_{i\downarrow} c_{j\uparrow} \right), \quad (4.1)$$

where $c^{\dagger}_{i\sigma}(c_{i\sigma})$ creates (annihilates) an electron with spin σ, t is the nearest-neighbor hopping amplitude and t' is the next-nearest hopping amplitude on a square lattice made of N sites with lattice spacing a, μ is the chemical potential, and ϕ_{ij} is the Peierls phase factor for hopping from site j to i [28]:

$$\phi_{ij} = \frac{2\pi}{\phi_0} \int_j^i \mathbf{A} \cdot \mathbf{dr}, \quad (4.2)$$

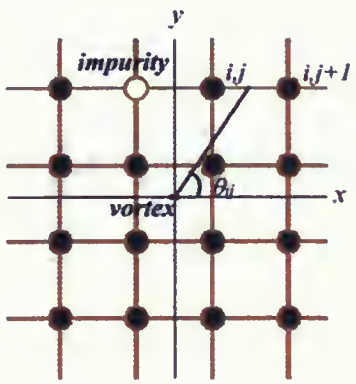

Figure 4.1: The definition of the angle θ in our lattice.

where $\phi_0 = hc/e$ is the flux quantum. We use the Landau gauge where $\mathbf{A} = By\mathbf{i}$, it is the same as (2.16) in the case where the magnetic field is in z direction. Since the quasiparticles $\Psi(\mathbf{r})$ are represented by an electron-hole Nambu spinor

$$\Psi(\mathbf{r}) = \begin{pmatrix} \Psi_\uparrow(\mathbf{r}) \\ \Psi_\downarrow^\dagger(\mathbf{r}) \end{pmatrix}, \tag{4.3}$$

as we have discussed in Chapter 2, it is more convenient to use the Nambu representation of the Hamiltonian. In that representation, the Hamiltonian is given by a 4×4 matrix:

$$\mathcal{H} = -\sum_{<ij>} C_i^\dagger h_{ij} C_j \tag{4.4}$$

where $C_i^\dagger = (c_{i\downarrow}^\dagger, c_{i\uparrow})$ and $C_j = (c_{j\uparrow}, c_{j\downarrow}^\dagger)^T$ are the Nambu creation and annihilation operators, and

$$h_{ij} = \begin{pmatrix} -t_{ij} - \mu\delta_{ij} & \Delta_{ij} \\ \Delta_{ij}^* & t_{ji} + \mu\delta_{ij} \end{pmatrix}, \tag{4.5}$$

is the BdG lattice Hamiltonian. The order parameter Δ_{ij} corresponding to $d_{x^2-y^2}$ symmetry is :

$$\Delta_{ij} = |\Delta_0| \exp(i\phi_{ij}) = |\Delta_0| \exp[i(\phi_0 + \theta_{ij})] \tag{4.6}$$

where the phase ϕ_0 is defined by

$$|\Delta_0| \exp(i\phi_0) = \begin{cases} \Delta_0 & \text{along x axis,} \\ -\Delta_0 & \text{along y axis,} \end{cases} \tag{4.7}$$

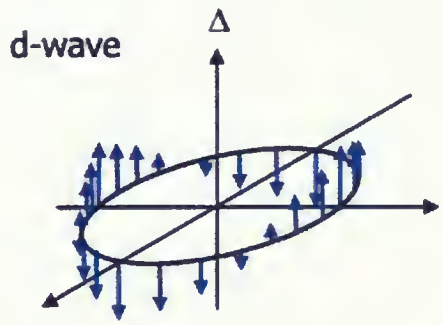

Figure 4.2: The order parameter in a d-wave superconductor.

The momentum representation of this expression is given by (3.9). Here Δ_0 is related to the rate at which the gap opens up at the nodes and we assume it as a constant, and as we have discussed in Chapter 2, θ_{ij} is the phase of superconducting electrons and varies by 2π in making a complete circle, corresponding to the existence of a single flux quantum associated with the vortex [2]. This phase can be represented in the form $\theta_{ij} = \arctan y/x$, where (x,y) is the coordination of the corresponding bond with respect to the vortex at the origin (Fig. 4.1). By using (4.6), one can plot Δ_{ij} in Fig. 4.2. The impurity scattering is described by the on-site scalar potential $U_{ij} = U\delta_{i,i0}\delta_{j,j0}$, where $(i0, j0)$ is the impurity position. This means that the potential U_{ij} is non-zero only at the position of the impurity.

4.2 Our model

In this section we explain the computational procedures used in calculating the interaction between vortex and impurity. The input parameters of the lattice BdG Hamiltonian (4.4) are chosen to comply with the literature values [29], so that meaningful comparisons could be made among the various works. The band parameters normalized to the nearest-neighbor hopping are $t'/t = -0.3$, $\mu/t = -1$, and the order parameter $\Delta_0/t = 0.04$. As we apply the magnetic field to the system, a single vortex appears on the lattice. In our model we put this vortex at the center of the lattice (Fig. 4.1), because it would decrease the possible numerical errors, and vary the impurity position.

First, we should initialize the Bogoliubov-De Gennes Hamiltonian for our 20×20 lattice, where

the matrix have 800 elements. For each position of the atom we can have two electrons for spin $\uparrow$ and spin $\downarrow$. We label these electrons by k, $k = 1$ for $\uparrow$ and $k = 2$ for $\downarrow$. Each electron is labeled by three factors, i, j, and k. For simplifying the problem we introduce new I. By using I we label the electrons from 1 to 800. For instance, $I = 1$ is for $i = 1$, $j = 1$, and $k = 1$. $I = 2$ is for $i = 1$, $j = 1$, and $k = 2$ and so on. Then I can be shown as

$$I = (2(i-1) \times 20) + (2(j-1) + k).$$

For each position of the electron on the lattice (I), there is an element for the system Hamiltonian. By using the tight binding model relations for a square lattice and the system BdG Hamiltonian, we can calculate all the elements of the Hamiltonian matrix for each position of impurity in our lattice. Suppose in our 20×20 square lattice, the electron jumps from the atom labeled I to the atom labeled I' which is its nearest neighbor the matrix element should be

$$t_{II'} = t \exp(i\phi_{II'}),$$

where

$$\phi_{II'} = \frac{2\pi}{\phi_0} \int_{I'}^{I} \mathbf{A} \cdot d\mathbf{r}.$$

As we have mentioned before, $\phi_0 = 2.07 \times 10^{-7}\ Ga/cm^2$ is the flux quantum. The applied magnetic field is in the $\mathbf{z}$ direction: $\mathbf{B} = B\hat{z}$. By using the Landau gauge, we can write

$$\phi_{II'} = \phi_0 \frac{\mathbf{A}_I - \mathbf{A}'_I}{2} (\mathbf{r}_I - \mathbf{r}'_I),$$

where $\mathbf{r}_I$ the distance the electron in I position to the vortex. By using $\mathbf{A} = \mathbf{i}Ba$, where the lattice constant $a = 1$ Å, and substituting it back to the equation and changing everything back to the old notation by using $I = I(i, j)$, we have

$$\phi_{II'} = \frac{2\pi}{\phi_0} \frac{(\mathbf{i}-1)Ba^2 + (\mathbf{i}'-1)Ba^2}{2} (\mathbf{j} - \mathbf{j}'),$$

so we can rewrite our $t's$ as

$$t_{II'} = t \exp\left[\frac{\pi Ba^2}{\phi_0} (\mathbf{i} + \mathbf{i}' - 2)(\mathbf{j} - \mathbf{j}')\right].$$

We now calculate the order parameter Δ_{ij}, by using (4.6) and (4.7). We calculate $t_{II'}$'s and Δ_{ij}'s for eight values of the magnetic field: $B = 0.1$ T, 0.2 T, 0.3 T, 0.4 T, 0.5 T, 0.6 T, 0.7 T, and 0.8 T, corresponding to the following values of the ratio : $Ba^2/\phi_0 = 1.0 \times 10^{-5}$, 2.0×10^{-5}, 3.0×10^{-5}, 4.0×10^{-5}, 5.0×10^{-5}, 6.0×10^{-5}, 7.0×10^{-5}, and 8.0×10^{-5}.

It is important to mention that we have to use an open boundary condition for our system. It is not possible to use the periodic boundary condition in our case, since the phase should vary by 2π in making a complete circle around the vortex. First we tried to use the periodic boundary condition but because the system is finite we had phase differences on the boundaries. Let us see in more detail what happens with the periodic boundary conditions. Suppose we look at an electron in position $(20, j)$ in a 20×20 lattice site. If we use the periodic boundary condition this electron should have the same hopping factor when it jumps to $(21, j)$ as $(1, j)$. But as we can see on Fig. 4.1, for an electron in position $(20, j)$, if the phase factor $\phi_{20j} = \theta_{20j}$, after hopping the phase factor for the electron is $\phi_{1j} = \pi - \theta_{20j}$. Our model must be continuous and the phase factor should not change when an electron jumps from site i to site $i + 1$. So the periodic boundary conditions do not work if there is only one vortex in the system.

In our model there is a single strong impurity, like Zn. Because of the energy gap anisotropy such impurity can cause a strong pair-breaking effect and we can choose the impurity potential as $U_{ij}/t = \delta_{i,i0}\delta_{j,j0}$ (here $(i0, j0)$ is the position of the impurity). We assume that the strength of the impurity is comparable to the bandwidth, i.e. $U_{i0,j0}/t = 1$. To measure the interaction between the impurity and the vortex in our system, we have changed the position of this impurity in the lattice. For different possible positions of the impurity we find the total energy of system by calculating the eigenvalues of the BdG Hamiltonian of the system at $T = 0$. Calculations are done both for the normal state E_n, when there is no vortex in the system, and the superconducting state E_s. After calculating the total energies, we calculate the difference between these two energies, E_n and E_s, and find ΔE for each position of the impurity:

$$\Delta E = (E_s - E_n) - E_{condensation}. \tag{4.8}$$

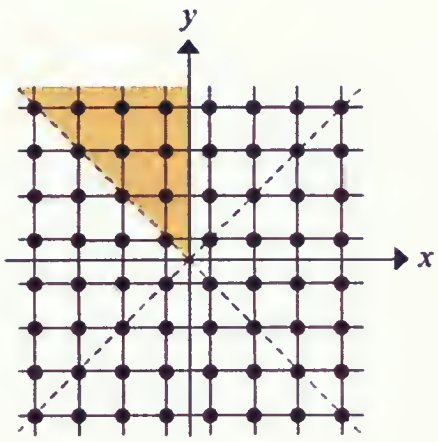

Figure 4.3: The square lattice in real space. The shaded region shows the different positions of the impurity that we have used for our calculations.

The condensation energy of electrons $E_{condensation}$ is defined by

$$E_{condensation} = E_s(\infty) - E_n(\infty), \tag{4.9}$$

i.e. as the difference in the total energy of the normal and the superconducting states for the furthest points from the vortex. In our case $E_n(\infty) = E_n(2)$ and $E_s(\infty) = E_s(2)$. We use $E_n(2)$ and $E_s(2)$ instead of $E_n(1)$ and $E_s(1)$ to minimize the numerical errors. We can change the position of the impurity and calculate ΔE's for different positions of the impurity. Because of the symmetry of the system, we can limit ourselves to the positions of the impurity in the shaded area in Fig. 4.3. Then we plot ΔE's with respect to the distance of the impurity from the vortex to find the interaction between vortex and impurity (the graphs are shown in the next Chapter).

There is always an upper limit on lattice size due to both the memory restrictions of the computing system and the run time of the programs. The total number of atoms for $N \times N$ lattice is N^2 which by considering the spin of electrons in the system the size of the Hamiltonian matrix that describes the system is $2N^2$. Clearly the memory required for the system is increasing rapidly as the size of the lattice is growing.

Chapter 5

Numerical Results and Discussion

In the previous Chapter we have explained in detail the computing procedure of the calculation of the interaction between impurity and vortex in our 20 × 20 lattice. The current Chapter presents the results of the calculations, accompanied by a general discussion and analysis of the data.

5.1 Results

As discussed in Chapter 4, we can calculate the total energy for normal state and superconducting state. The energy difference between normal and superconducting state is the condensation energy. We can calculate the condensation energies (ΔE's), for different positions of the impurity in our model (the shaded area in Fig. 4.3) and plot its distributions with respect to the position of the impurity for different applied magnetic fields.

Let us discuss one case in more detail. Consider the 20 × 20 lattice in an applied 0.2 T magnetic field. Fig. 5.1 shows the condensation energy of the model with respect to the different positions of the impurity. As we can see on Fig. 5.1, as the impurity gets closer to the vortex, the condensation energy gets lower. This shows that the position of the vortex is most likely close to the position of the impurity. In the normal case when there is no vortex in our system the total energy of the system for different positions of the impurity is shown in Fig. 5.2. Using a finite model and choosing the open boundary condition causes some errors, especially on the boundaries. When the system goes to it the superconducting state, by considering the vortex at the center of the model, the total energy for different positions of the impurities can be shown as Fig. 5.3.

Fig. 5.1 to Fig. 5.10 show the condensation energy for the 20 × 20 lattice for different applied magnetic fields. As we can see it is not clear if the lower condensation energy is at the center of the model. We do not calculate the energies at the boundaries because of the errors caused by using

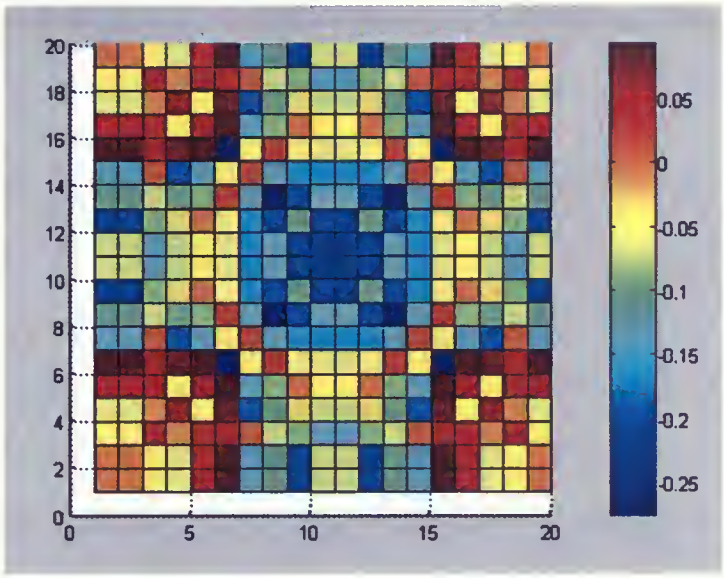

Figure 5.1: Condensation energy for 20 × 20 lattice, B=0.2 T

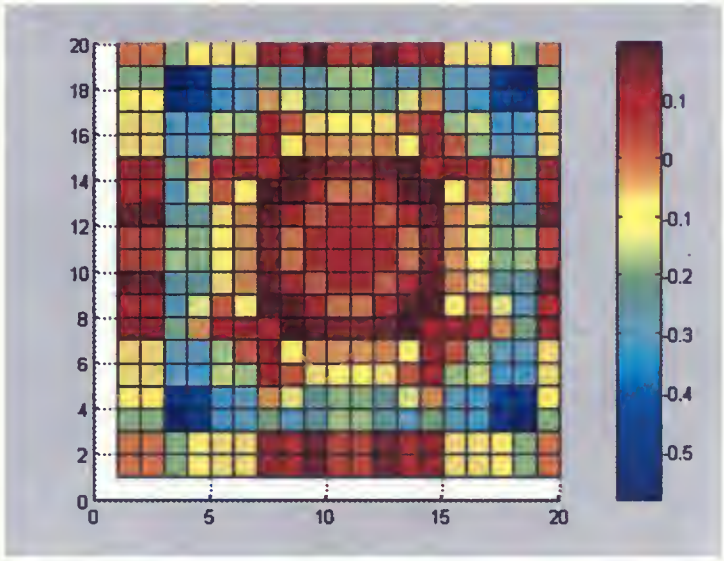

Figure 5.2: Total energy for normal state for 20 × 20 lattice, B=0.2 T

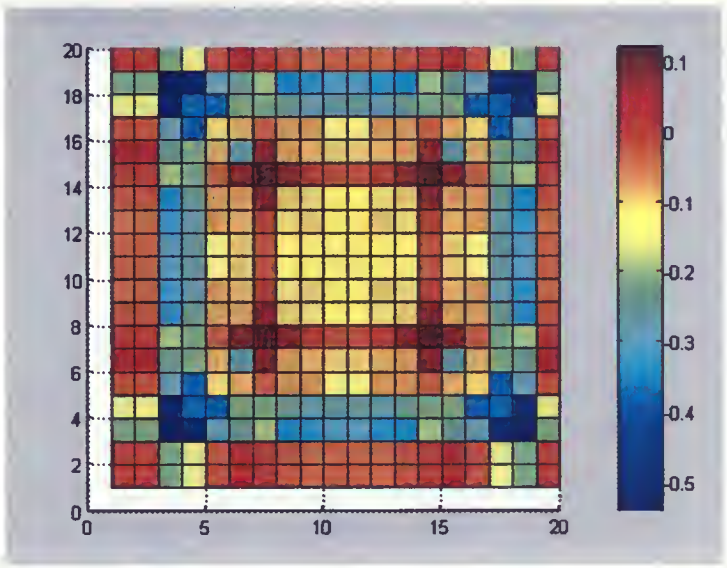

Figure 5.3: Total energy for superconducting state for 20 × 20 lattice, B=0.2 T

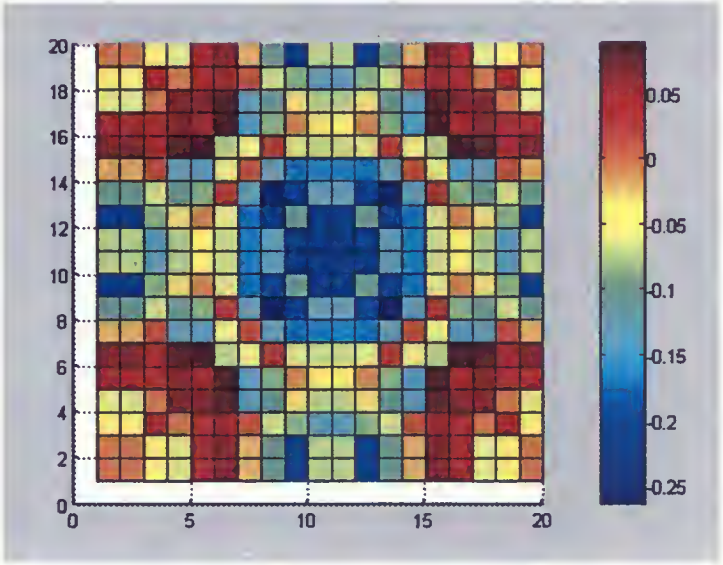

Figure 5.4: Condensation energy for 20 × 20 lattice, B=0.1 T

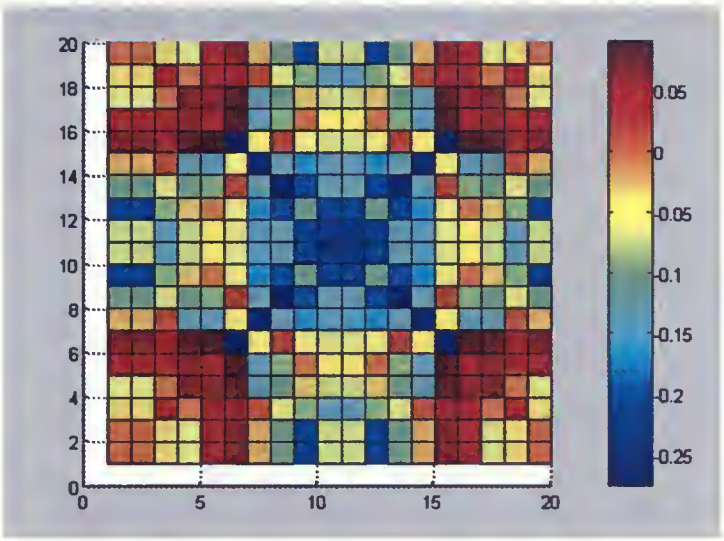

Figure 5.5: Condensation energy for 20 × 20 lattice, B=0.3 T

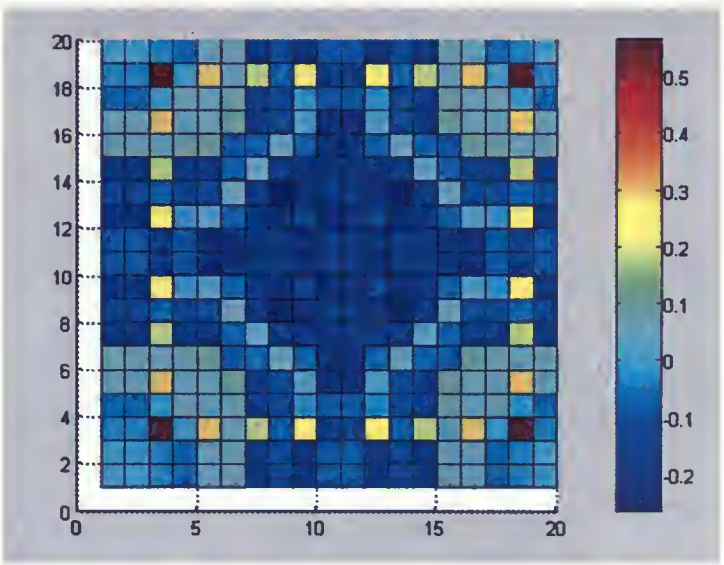

Figure 5.6: Condensation energy for 20 × 20 lattice site, B=0.4 T

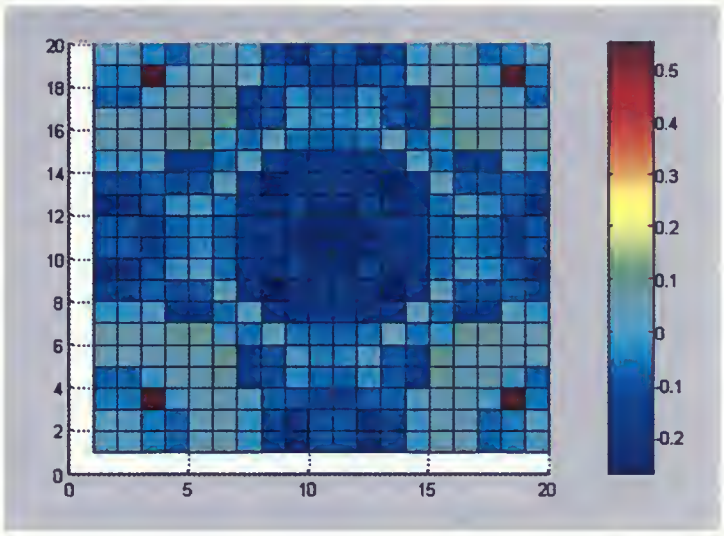

Figure 5.7: Condensation energy for 20 × 20 lattice, B=0.5 T

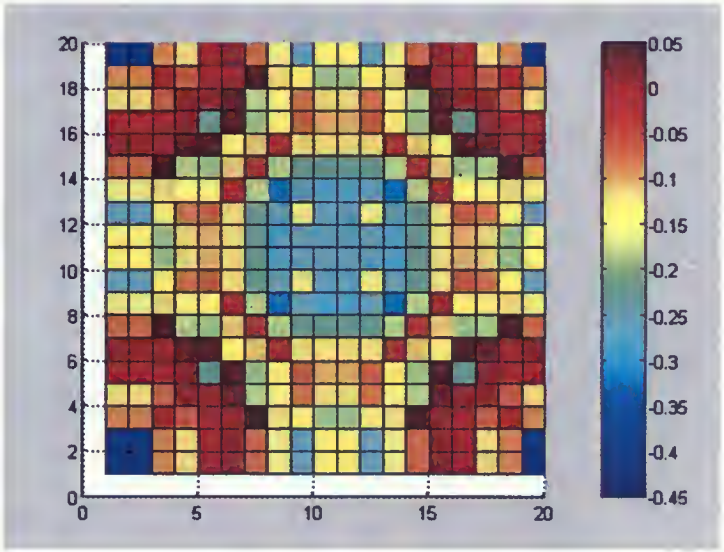

Figure 5.8: Condensation energy for 20 × 20 lattice, B=0.6 T

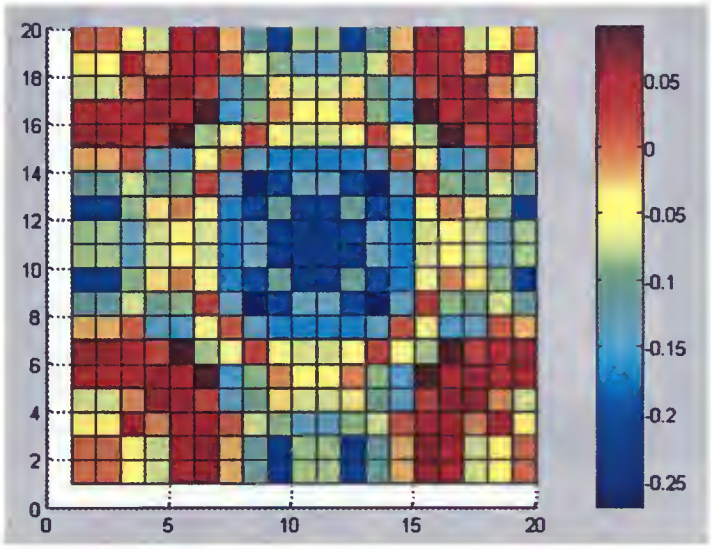

Figure 5.9: Condensation energy for 20 × 20 lattice, B=0.7 T

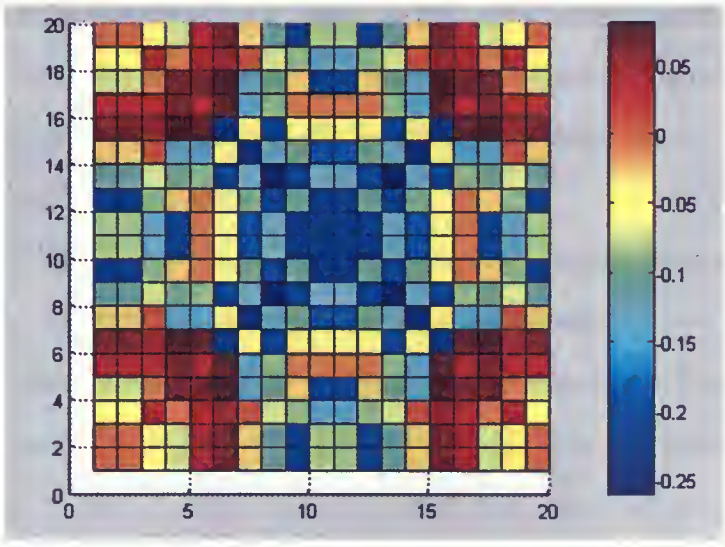

Figure 5.10: Condensation energy for 20 × 20 lattice, B=0.8 T

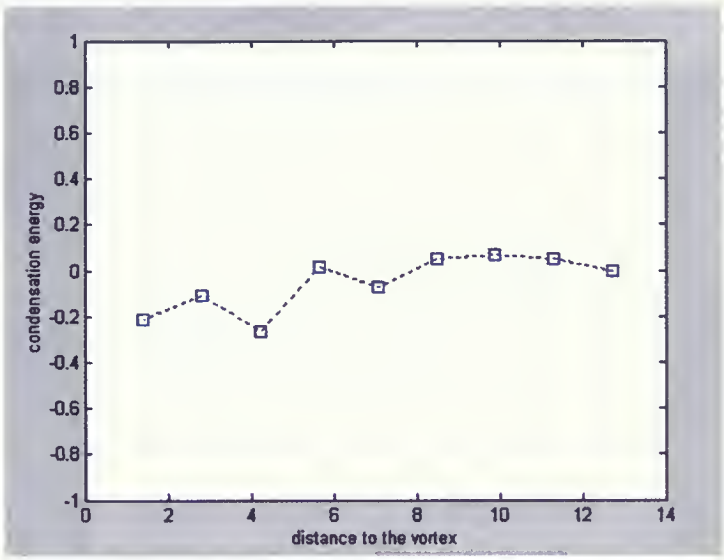

Figure 5.11: Condensation energy for B=0.1 T vs. distance to the vortex along the diagonal for 20 × 20 lattice.

the open boundary condition.

To have a better understanding of the changes of the condensation energy for different positions of the impurity, first we plot the changes of the condensation energy for each value of the magnetic field vs. the distance of the atoms on the diagonal to the vortex at the center of the 20 × 20 lattice (Fig. 5.11 to Fig. 5.18). Next we consider the impurities along the y axis for each value of the magnetic field and again plot the changes of the condensation energy vs. the distance to the vortex for these atoms (Fig. 5.19 to Fig. 5.26).

As we can see from Fig. 5.11 to Fig. 5.18, when we are changing the position of the impurity along the diagonal, the condensation energy shows some decreasing behavior as the position of the impurity gets closer to the vortex. Fig. 5.19 to Fig. 5.26 does not show a clear decreasing behavior for the condensation energy of the impurities along the y axis when the impurity gets closer to the vortex.

We have used the same algorithm for calculating the condensation energy distribution for a 24 × 24 lattice as well as a 30 × 30 lattice when the applied magnetic field is 0.2 T (Fig. 5.27 and Fig. 5.28).

As we can see from Fig. 5.27 for a 24 × 24 lattice, the condensation energy has its minimum value

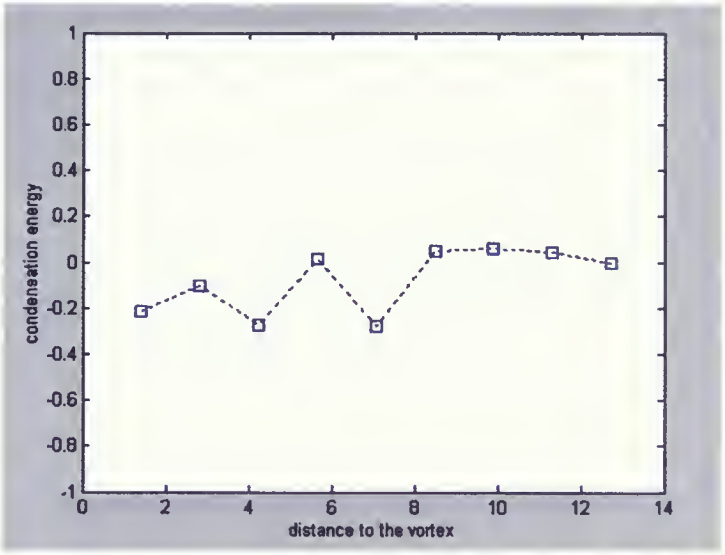

Figure 5.12: Condensation energy for B=0.2 T vs. distance to the vortex along the diagonal for 20 × 20 lattice.

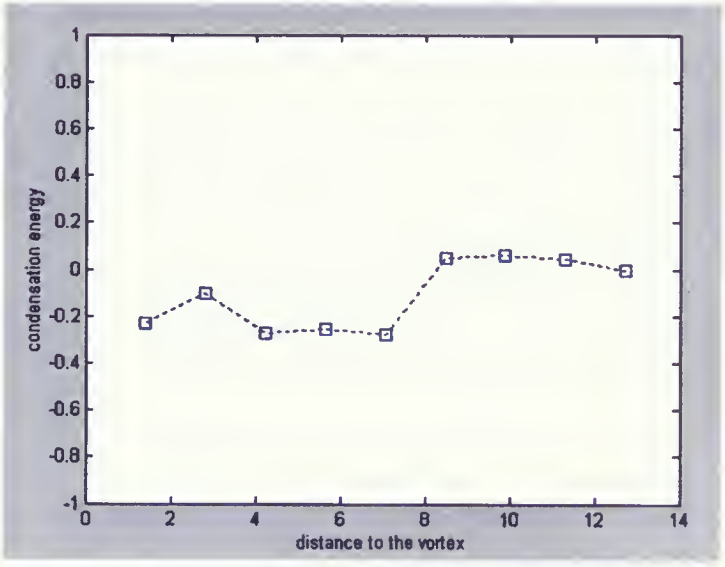

Figure 5.13: Condensation energy for B=0.3 T vs. distance to the vortex along the diagonal for 20 × 20 lattice.

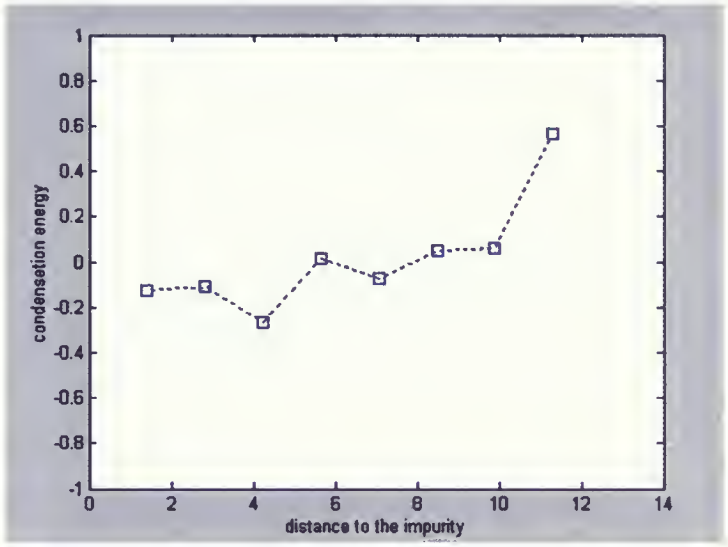

Figure 5.14: Condensation energy for B=0.4 T vs. distance to the vortex along the diagonal for 20 × 20 lattice.

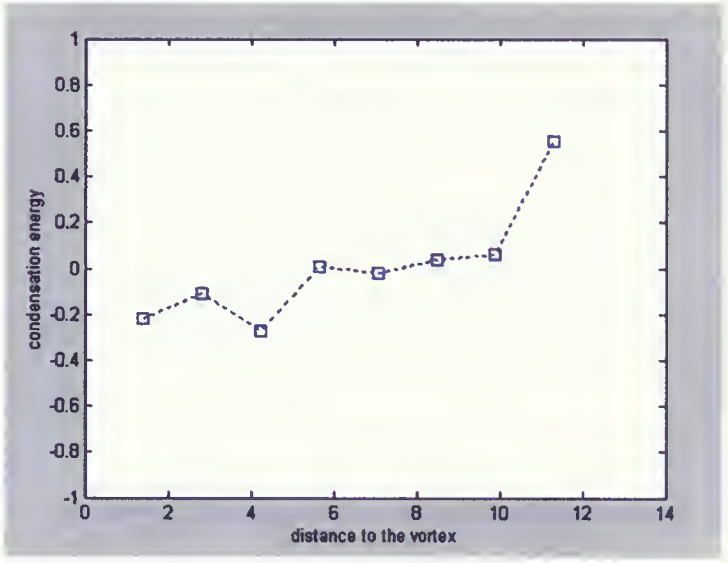

Figure 5.15: Condensation energy for B=0.5 T vs. distance to the vortex along the diagonal for 20 × 20 lattice.

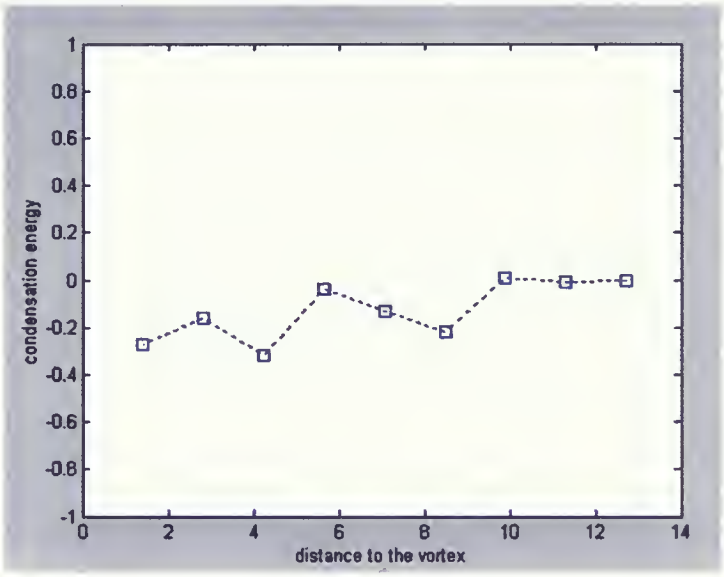

Figure 5.16: Condensation energy for B=0.6 T vs. distance to the vortex along the diagonal for 20 × 20 lattice.

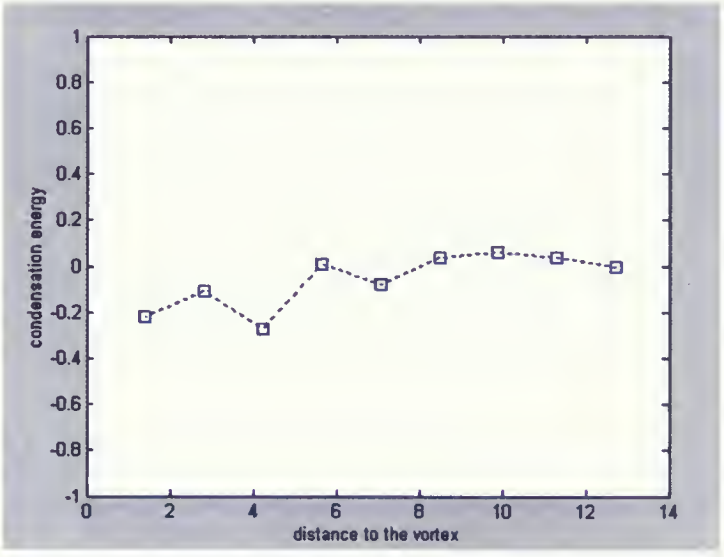

Figure 5.17: Condensation energy for B=0.7 T vs. distance to the vortex along the diagonal for 20 × 20 lattice.

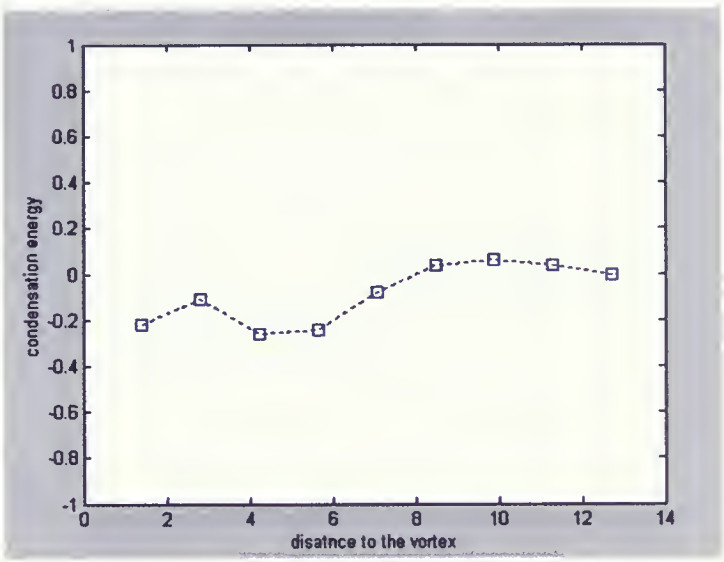

Figure 5.18: Condensation energy for B=0.8 T vs. distance to the vortex along the diagonal for 20 × 20 lattice.

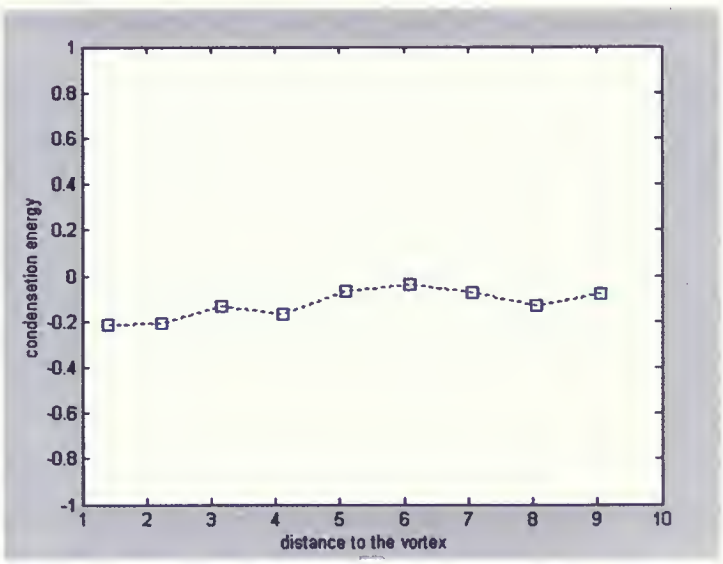

Figure 5.19: Condensation energy for B=0.1 T vs. distance to the vortex along the y axis for 20 × 20 lattice.

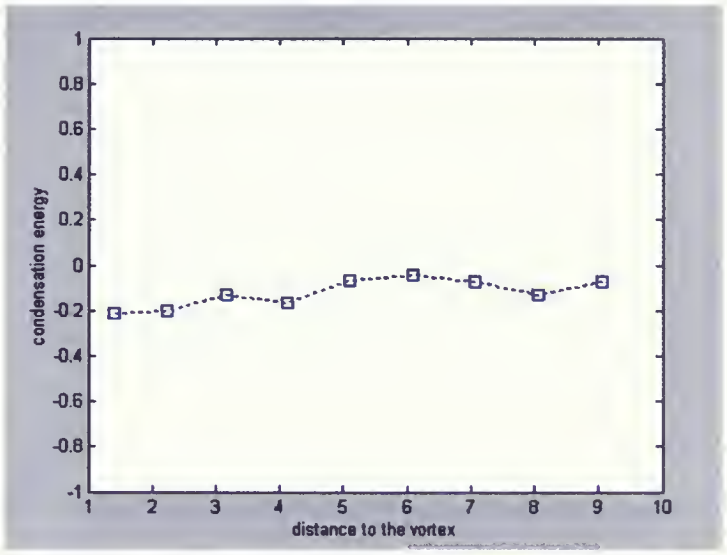

Figure 5.20: Condensation energy for B=0.2 T vs. distance to the vortex along the y axis for 20 × 20 lattice.

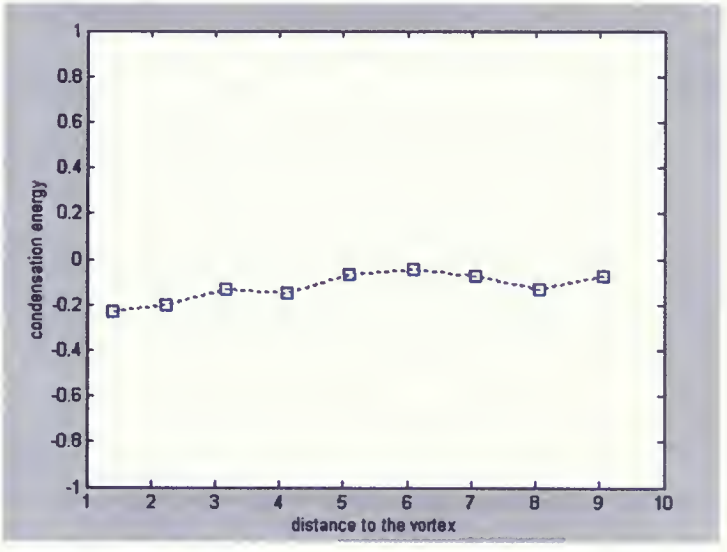

Figure 5.21: Condensation energy for B=0.3 T vs. distance to the vortex along the y axis for 20 × 20 lattice.

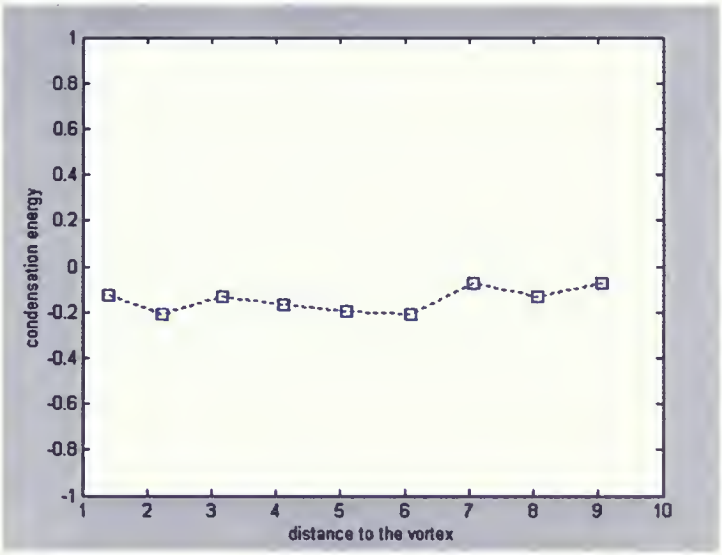

Figure 5.22: Condensation energy for B=0.4 T vs. distance to the vortex along the y axis for 20 × 20 lattice.

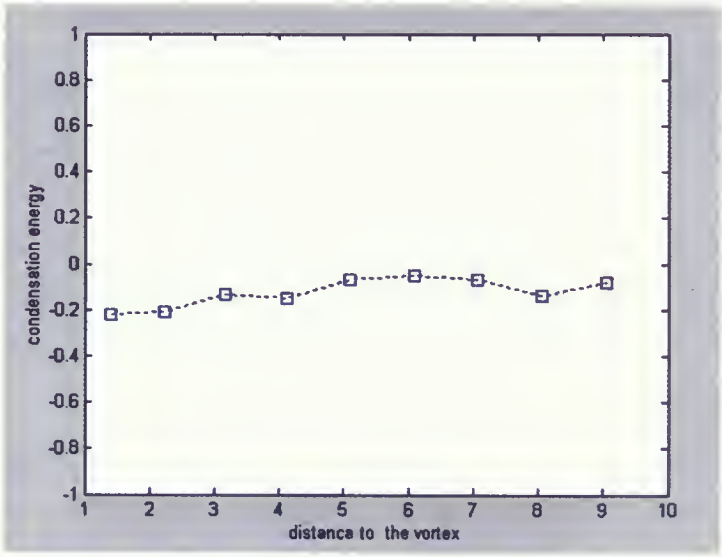

Figure 5.23: Condensation energy for B=0.5 T vs. distance to the vortex along the y axis for 20 × 20 lattice.

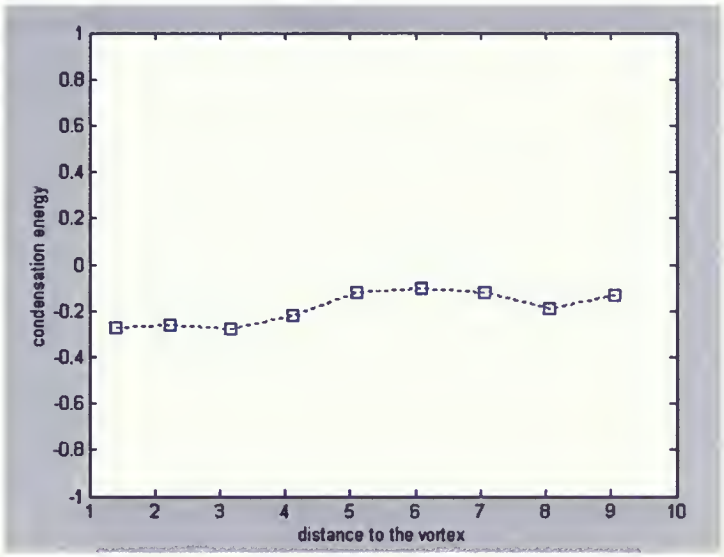

Figure 5.24: Condensation energy for B=0.6 T vs. distance to the vortex along the y axis for 20 × 20 lattice.

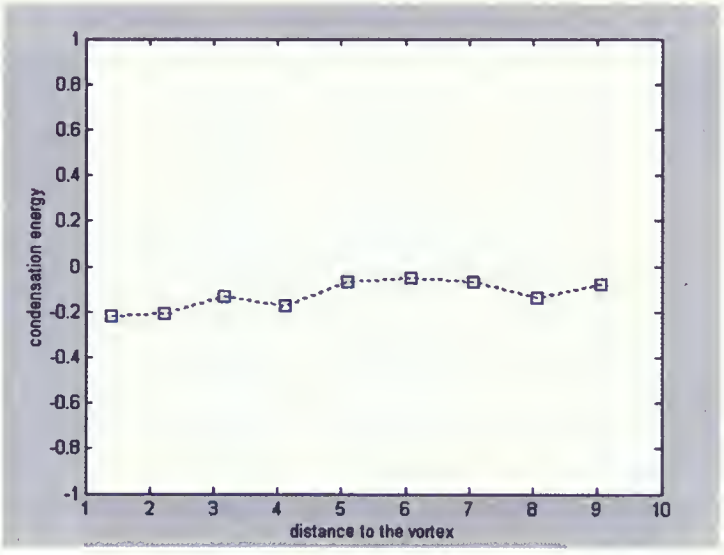

Figure 5.25: Condensation energy for B=0.7 T vs. distance to the vortex along the y axis for 20 × 20 lattice.

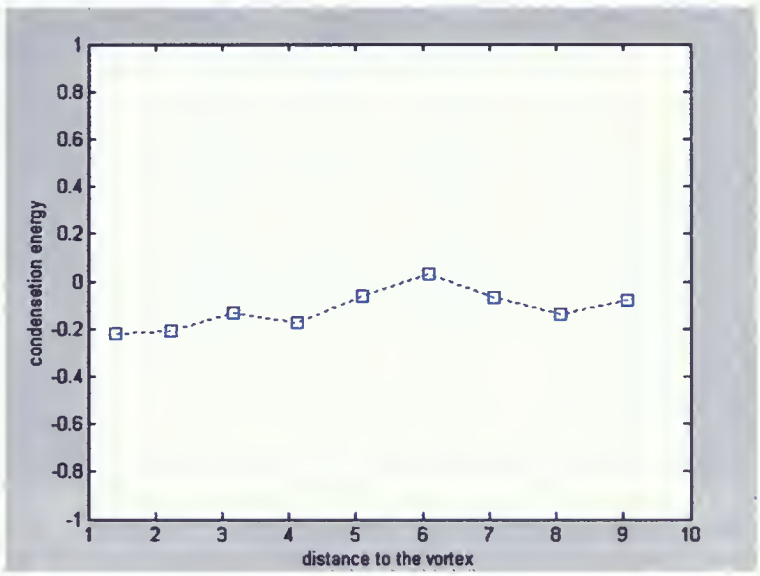

Figure 5.26: Condensation energy for B=0.8 T vs. distance to the vortex along the y axis for 20 × 20 lattice.

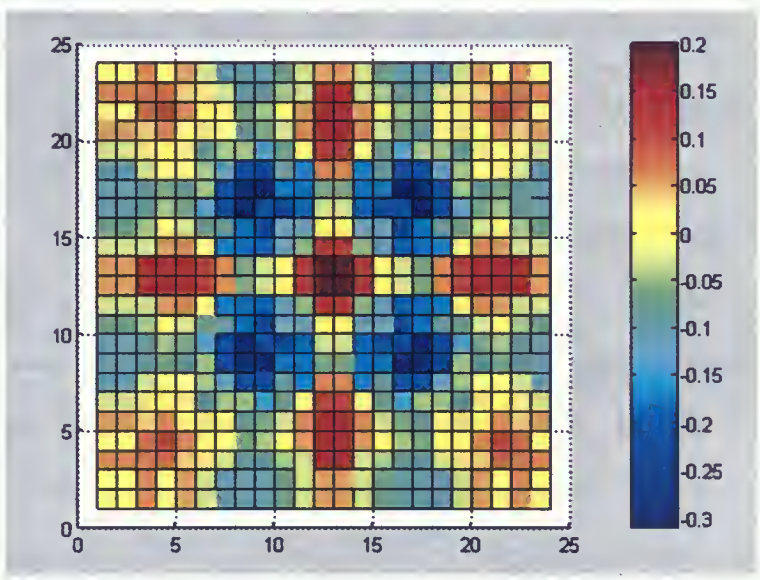

Figure 5.27: Condensation energy for 24 × 24 lattice, B=0.2 T

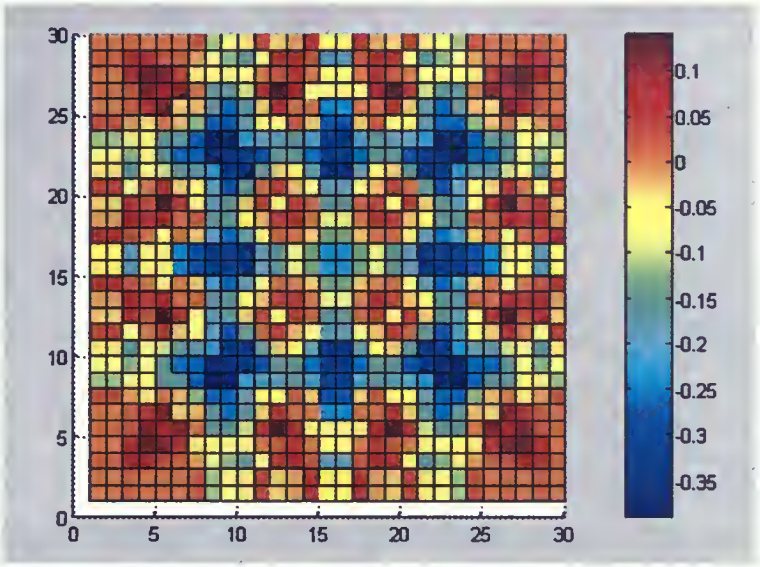

Figure 5.28: Condensation energy for 30 × 30 lattice, B=0.2 T

somewhere between the vortex position and the edge of the sample along the diagonal. Although the condensation energy for 30 × 30 lattice, Fig. 5.28, has a minimum value at the center but there are some other areas that show the minimum condensation energies.

5.2 Conclusions

In conclusion, this thesis has focused on the calculation of the interaction between vortices and impurities in a d-wave superconductor mostly by using the observations of Davis *et* al. [15] on BSCCO. To make the study as comprehensive as possible, we apply different magnetic fields and change the position of the single impurity in our model. The calculations for eight different values of the magnetic field show that there is no clear relation between the condensation energy of the system and the position of the impurity relative to the vortex. In other words, our results can not explain the experimental fact that the vortices are attracted to strong impurities in d-wave superconductors. It might be due to the fact that the size of our model is insufficient and we are using open boundary conditions.

Appendix A

Program code

The program initializes the elements of the Bogoliubov-de Gennes Hamiltonian for an 800 × 800 matrix related to a 20 × 20 lattice for each position of the impurity on the lattice. Generally the program is set to calculate the eigenvalue problem of the Hamiltonian and find the eigenvalues both for normal state and superconducting state for each position of the impurity.

First we introduce the constant values that have been chosen for our calculations (see Chapter 4) and the program requires the dimensionality of the lattice. Next we have six "for" loops for introducing the position of each atom and its nearest neighbor or next nearest neighbor atom. Now we start to introduce each element of the matrix. We have several "if" conditions; we have a chemical potential, μ/t=-1, for any atom except the impurity. The impurity has the potential $U_{i0,j0}$/t=1. The next two "if's" calculate the elements of the matrix for nearest neighbor hoppings along the y axis. Then we calculate the elements of the matrix for the nearest neighbor hoppings along the x axis. Then it is time to calculate the matrix elements for next nearest neighbor hoppings. After calculating the tight-binding elements, we should calculate $\Delta's$. For the normal state, since $\Delta = 0$, other matrix elements are zero. For superconducting state, $\Delta_0 = 0.04$ and the remaining if's will calculate the $\Delta's$ by calculating the phase factor for each bond. After initializing the matrix elements, the program calculates the eigenvalue problem. By using the eigenvalues it calculates the total energy of the system both for normal and superconducting states. We continue these calculations for each position of the impurity and for different values of the magnetic field.

```
%-------------------------------------------------------------
% The values that I am using
%-------------------------------------------------------------

Baaofi=4*0.00001;          %--------- magnetic field B, times a squared times phi
cons=(2*pi*(Baaofi));
t0=1;                      %--------- t0 is is the nearest neighbor hopping amplitude
Delta=0.04;                %--------- Delta is the order parameter
t1=-0.3;                   %--------- t1 is the next nearest neighbor hopping amplitude
mu=-1;                     %--------- mu is the chemical potential
a=0.0000000001;            %--------- a is the lattice constant
cnt=1;
N=input('what is N? ')     %--------- N is the dimension of the matrix

%-------------------------------------------------------------
% For Elements
%-------------------------------------------------------------


for (i=1:1:N),
for (j=1:1:N),
for (k=1:1:2),
I=((2*(i-1)*N)+(2*(j-1)+k));    %--------- label atoms by I
for (ii=1:1:N),
for (jj=1:1:N),
for (kk=1:1:2),
II=((2*(ii-1)*N)+(2*(jj-1)+kk)); %--------- label targets by II


%-------------------------------------------------------------
% Matrix Elements
%-------------------------------------------------------------

%-------------------------------------------------------------
%Conditrion for the chemical potential. The impurity is in position (10,10)
%the U/t0=1
%-------------------------------------------------------------

if((k==kk)&(i~=10)&(j~=10)&(jj==j)&(i==ii))
t=mu/t0;

%-------------------------------------------------------------
%nearest neighbors
%-------------------------------------------------------------
%#along y axis
```

```
else if ((k==kk)&(j==jj)&(ii==(i-1))&(i~=1))
t=1;

else if((k==kk)&(j==jj)&(ii==(i+1)))
t=1;
%-------------------------------------------------------------
%#along x axis

else if((k==kk)&(jj==j+1)&(i==ii))
t=(t0*(complex(cos(cons*(i+ii-2)*(j-jj)),sin(cons*(i+ii-2)*(j-jj)))))/t0;

else if((k==kk)&(jj==j-1)&(i==ii))
t=(t0*(complex(cos(cons*(i+ii-2)*(j-jj)),sin(cons*(i+ii-2)*(j-jj)))))/t0;

%-------------------------------------------------------------
%next nearest neighbors
%-------------------------------------------------------------

else if((k==kk)&(jj==j+1)&(ii==i+1))
t=(t1*(complex(cos(cons*(i+ii-2)*(j-jj)),sin(cons*(i+ii-2)*(j-jj)))))/t0;

else if((k==kk)&(jj==j-1)&(ii==i-1))
t=(t1*(complex(cos(cons*(i+ii-2)*(j-jj)),sin(cons*(i+ii-2)*(j-jj)))))/t0;

else if((k==kk)&(jj==j+1)&(ii==i-1))
t=(t1*(complex(cos(cons*(i+ii-2)*(j-jj)),sin(cons*(i+ii-2)*(j-jj)))))/t0;

else if((k==kk)&(jj==j-1)&(ii==i+1))
t=(t1*(complex(cos(cons*(i+ii-2)*(j-jj)),sin(cons*(i+ii-2)*(j-jj)))))/t0;

%-------------------------------------------------------------
% Conditions on Deltas (with single Vortex )
%-------------------------------------------------------------

%-------------------------------------------------
% theta is between 0 to pi/2
%-------------------------------------------------

%-------------------------------------------------------------
%i<=N/2 & j>=(N/2+1) because we are looking for phase defferences from 0 to pi/2
%-------------------------------------------------------------

else if((i<=N/2)&(j>=(N/2+1))&(k==1)&(ii==i)&(jj==j+1)&(kk==2))
x=(jj-(N/2+1))*a; y=(((N+1)/2)-i)*a; theta=(atan(y/x));

phase=(complex(cos(theta),sin(theta)));
```

```
t=((Delta)*(phase))/t0;

else if((i<=N/2)&(j>=(N/2+1))&(k==2)&(ii==i)&(jj==j+1)&(kk==1))
x=(jj-(N/2+1))*a; y=(((N+1)/2)-i)*a; theta=(atan(y/x));

phase=(complex(cos(theta),-sin(theta)));
t=((Delta)*(phase))/t0;

else if((i<=N/2)&(j>=(N/2+2))&(k==1)&(ii==i)&(jj==j-1)&(kk==2))
x=(j-(N/2+1))*a; y=(((N+1)/2)-i)*a; theta=(atan(y/x));

phase=(complex(cos(theta),sin(theta)));
t=((Delta)*(phase))/t0;

else if((i<=N/2)&(j>=(N/2+2))&(k==2)&(ii==i)&(jj==j-1)&(kk==1))
x=(j-(N/2+1))*a; y=(((N+1)/2)-i)*a; theta=(atan(y/x));

phase=(complex(cos(theta),-sin(theta)));
t=((Delta)*(phase))/t0;

else if((i<=(N/2-1))&(j>=(N/2+1))&(k==1)&(ii==i+1)&(jj==j)&(kk==2))
x=(j-((N+1)/2))*a; y=((N/2+1)-ii)*a; theta=(atan(y/x));

phase=(complex(cos(theta),sin(theta)));
t=-((Delta)*(phase))/t0;

else if((i<=(N/2-1))&(j>=(N/2+1))&(k==2)&(ii==i+1)&(jj==j)&(kk==1))
x=(j-((N+1)/2))*a; y=((N/2+1)-ii)*a; theta=(atan(y/x));

phase=(complex(cos(theta),-sin(theta)));
t=-((Delta)*(phase))/t0;

else if((i<=N/2)&(j>=(N/2+1))&(k==1)&(kk==2)&(jj==j)&(ii==i-1))
x=(j-((N+1)/2))*a; y=((N/2+1)-i)*a; theta=(atan(y/x));

phase=(complex(cos(theta),sin(theta)));
t=-((Delta)*(phase))/t0;

else if((i<=N/2)&(j>=(N/2+1))&(k==2)&(kk==1)&(jj==j)&(ii==i-1))
x=(j-((N+1)/2))*a; y=((N/2+1)-i)*a; theta=(atan(y/x));

phase=(complex(cos(theta),-sin(theta)));
t=-((Delta)*(phase))/t0;

%-------------------------------------------------
% theta is 2pi
```

```
%-------------------------------------------------

%-------------------------------------------------------------
%j==N/2 & i<=N/2 because we are looking for the phase difference pi/2
%-------------------------------------------------------------

else if((i<=N/2)&(j==N/2)&(k==1)&(ii==i)&(jj==(N/2+1))&(kk==2))
theta=(pi/2);

phase=(complex(cos(theta),sin(theta)));
t=((Delta)*(phase))/t0;

else if((i<=N/2)&(j==N/2)&(k==2)&(ii==i)&(jj==(N/2+1))&(kk==1))
theta=(pi/2);

phase=(complex(cos(theta),-sin(theta)));
t=((Delta)*(phase))/t0;

else if((i<=N/2)&(j==(N/2+1))&(k==1)&(ii==i)&(jj==N/2)&(kk==2))
theta=(pi/2);

phase=(complex(cos(theta),sin(theta)));
t=((Delta)*(phase))/t0;

else if((i<=N/2)&(j==(N/2+1))&(k==2)&(ii==i)&(jj==N/2)&(kk==1))
theta=(pi/2);

phase=(complex(cos(theta),-sin(theta)));
t=((Delta)*(phase))/t0;

%-------------------------------------------------
%  theta is between pi/2 to pi
%-------------------------------------------------


%-------------------------------------------------------------
% i<=N/2 & j<=N/2 we are looking for phase differences from pi/2 to pi
%-------------------------------------------------------------

else if((i<=N/2)&(j<=(N/2-1))&(k==1)&(ii==i)&(jj==j+1)&(kk==2))
x=((N/2+1)-jj)*a; y=(((N+1)/2)-i)*a; theta=(pi-(atan(y/x)));

phase=(complex(cos(theta),sin(theta)));
t=((Delta)*(phase))/t0;

else if((i<=N/2)&(j<=(N/2-1))&(k==2)&(ii==i)&(jj==j+1)&(kk==1))
```

```
x=((N/2+1)-jj)*a; y=(((N+1)/2)-i)*a; theta=(pi-(atan(y/x)));

phase=(complex(cos(theta),-sin(theta)));
t=((Delta)*(phase))/t0;

else if((i<=N/2)&(j<=N/2)&(k==1)&(ii==i)&(jj==j-1)&(kk==2))
x=((N/2+1)-j)*a; y=(((N+1)/2)-i)*a; theta=(pi-(atan(y/x)));

phase=(complex(cos(theta),sin(theta)));
t=((Delta)*(phase))/t0;

else if((i<=N/2)&(j<=N/2)&(k==2)&(ii==i)&(jj==j-1)&(kk==1))
x=((N/2+1)-j)*a; y=(((N+1)/2)-i)*a; theta=(pi-(atan(y/x)));

phase=(complex(cos(theta),-sin(theta)));
t=((Delta)*(phase))/t0;

else if((i<=(N/2-1))&(j<=N/2)&(k==1)&(ii==i+1)&(jj==j)&(kk==2))
x=(((N+1)/2)-j)*a; y=((N/2+1)-ii)*a; theta=(pi-(atan(y/x)));

phase=(complex(cos(theta),sin(theta)));
t=-((Delta)*(phase))/t0;

else if((i<=(N/2-1))&(j<=N/2)&(k==2)&(ii==i+1)&(jj==j)&(kk==1))
x=(((N+1)/2)-j)*a; y=((N/2+1)-ii)*a; theta=(pi-(atan(y/x)));

phase=(complex(cos(theta),-sin(theta)));
t=-((Delta)*(phase))/t0;

else if((i<=N/2)&(j<=N/2)&(k==1)&(ii==i-1)&(jj==j)&(kk==2))
x=(((N+1)/2)-j)*a; y=((N/2+1)-i)*a; theta=(pi-(atan(y/x)));

phase=(complex(cos(theta),sin(theta)));
t=-((Delta)*(phase))/t0;

else if((i<=N/2)&(j<=N/2)&(k==2)&(ii==i-1)&(jj==j)&(kk==1))
x=(((N+1)/2)-j)*a; y=((N/2+1)-i)*a; theta=(pi-(atan(y/x)));

phase=(complex(cos(theta),-sin(theta)));
t=-((Delta)*(phase))/t0;

%-------------------------------------------------
%  theta is pi
%-------------------------------------------------

%-------------------------------------------------------
```

```
%i==N/2 & j<=N/2 because we are looking for the phase difference pi
%-----------------------------------------------------------

else if((i==N/2)&(j<=N/2)&(k==1)&(ii==(N/2+1))&(jj==j)&(kk==2))
theta=(pi);

phase=(complex(cos(theta),sin(theta)));
t=-((Delta)*(phase))/t0;

else if((i==N/2)&(j<=N/2)&(k==2)&(ii==(N/2+1))&(jj==j)&(kk==1))
theta=(pi);

phase=(complex(cos(theta),-sin(theta)));
t=-((Delta)*(phase))/t0;

else if((i==(N/2+1))&(j<=N/2)&(k==1)&(ii==N/2)&(jj==j)&(kk==2))
theta=(pi);

phase=(complex(cos(theta),sin(theta)));
t=-((Delta)*(phase))/t0;

else if((i==(N/2+1))&(j<=N/2)&(k==2)&(ii==N/2)&(jj==j)&(kk==1))
theta=(pi);

phase=(complex(cos(theta),-sin(theta)));
t=-((Delta)*(phase))/t0;

%-------------------------------------------------
%  theta is between pi to 3pi/2
%-------------------------------------------------

%-----------------------------------------------------------
% i>=N/2 & j<=N/2 because we are looking for the phase differences from pi to 3pi/2
%-----------------------------------------------------------

else if((i>=(N/2+1))&(j<=(N/2-1))&(k==1)&(ii==i)&(jj==j+1)&(kk==2))
x=((N/2+1)-jj)*a; y=(i-((N+1)/2))*a; theta=(pi-(atan(y/x)));

phase=(complex(cos(theta),sin(theta)));
t=((Delta)*(phase))/t0;

else if((i>=(N/2+1))&(j<=(N/2-1))&(k==2)&(ii==i)&(jj==j+1)&(kk==1))
x=((N/2+1)-jj)*a; y=(i-((N+1)/2))*a; theta=(pi-(atan(y/x)));

phase=(complex(cos(theta),-sin(theta)));
t=((Delta)*(phase))/t0;
```

```
else if((i>=(N/2+1))&(j<=N/2)&(k==1)&(ii==i)&(jj==j-1)&(kk==2))
x=((N/2+1)-j)*a; y=(i-((N+1)/2))*a; theta=(pi-(atan(y/x)));

phase=(complex(cos(theta),sin(theta)));
t=((Delta)*(phase))/t0;

else if((i>=(N/2+1))&(j<=N/2)&(k==2)&(ii==i)&(jj==j-1)&(kk==1))
x=((N/2+1)-j)*a; y=(i-((N+1)/2))*a; theta=(pi-(atan(y/x)));

phase=(complex(cos(theta),-sin(theta)));
t=-((Delta)*(phase))/t0;

else if((i>=(N/2+1))&(j<=N/2)&(k==1)&(ii==i+1)&(jj==j)&(kk==2))
x=(((N+1)/2)-j)*a; y=(ii-(N/2+1))*a; theta=(pi-(atan(y/x)));

phase=(complex(cos(theta),sin(theta)));
t=-((Delta)*(phase))/t0;

else if((i>=(N/2+1))&(j<=N/2)&(k==2)&(ii==i+1)&(jj==j)&(kk==1))
x=(((N+1)/2)-j)*a; y=(ii-(N/2+1))*a; theta=(pi-(atan(y/x)));

phase=(complex(cos(theta),-sin(theta)));
t=-((Delta)*(phase))/t0;

else if((i>=(N/2+2))&(j<=N/2)&(k==1)&(ii==i-1)&(jj==j)&(kk==2))
x=(((N+1)/2)-j)*a; y=(i-(N/2+1))*a; theta=(pi-(atan(y/x)));

phase=(complex(cos(theta),sin(theta)));
t=-((Delta)*(phase))/t0;

else if((i>=(N/2+2))&(j<=N/2)&(k==2)&(ii==i-1)&(jj==j)&(kk==1))
x=(((N+1)/2)-j)*a; y=(i-(N/2+1))*a; theta=(pi-(atan(y/x)));

phase=(complex(cos(theta),-sin(theta)));
t=-((Delta)*(phase))/t0;

%-------------------------------------------------
%  theta is 3pi/2
%-------------------------------------------------

%-----------------------------------------------------------
%i>=N/2 & j==N/2 because we are looking for the phase difference 3pi/2
%-----------------------------------------------------------

else if((i>=(N/2+1))&(j==N/2)&(k==1)&(ii==i)&(jj==(N/2+1))&(kk==2))
```

```
theta=((3*pi)/2);

phase=(complex(cos(theta),sin(theta)));
t=((Delta)*(phase))/t0;

else if((i>=(N/2+1))&(j==N/2)&(k==2)&(ii==i)&(jj==(N/2+1))&(kk==1))
theta=((3*pi)/2);

phase=(complex(cos(theta),-sin(theta)));
t=((Delta)*(phase))/t0;

else if((i>=(N/2+1))&(j==(N/2+1))&(k==1)&(ii==i)&(jj==N/2)&(kk==2))
theta=((3*pi)/2);

phase=(complex(cos(theta),sin(theta)));
t=((Delta)*(phase))/t0;

else if((i>=(N/2+1))&(j==(N/2+1))&(k==2)&(ii==i)&(jj==N/2)&(kk==1))
theta=((3*pi)/2);

phase=(complex(cos(theta),-sin(theta)));
t=((Delta)*(phase))/t0;

%-------------------------------------------------
%  theta is between 3pi/2 to 2pi
%-------------------------------------------------

%-----------------------------------------------------------
%i>=N/2 & j>=N/2 because we are looking for the phase differences from 3pi/2 to 2pi
%-----------------------------------------------------------

else if((i>=(N/2+1))&(j>=(N/2+1))&(k==1)&(ii==i)&(jj==j+1)&(kk==2))
x=(jj-(N/2+1))*a; y=(i-((N+1)/2))*a; theta=((2*pi)-atan(y/x));

phase=(complex(cos(theta),sin(theta)));
t=((Delta)*(phase))/t0;

else if((i>=(N/2+1))&(j>=(N/2+1))&(k==2)&(ii==i)&(jj==j+1)&(kk==1))
x=(jj-(N/2+1))*a; y=(i-((N+1)/2))*a; theta=((2*pi)-atan(y/x));

phase=(complex(cos(theta),-sin(theta)));
t=((Delta)*(phase))/t0;

else if((i>=(N/2+1))&(j>=(N/2+2))&(k==1)&(ii==i)&(jj==j-1)&(kk==2))
x=(j-(N/2+1))*a; y=(i-((N+1)/2))*a; theta=((2*pi)-atan(y/x));
```

```
phase=(complex(cos(theta),sin(theta)));
t=((Delta)*(phase))/t0;

else if((i>=(N/2+1))&(j>=(N/2+2))&(k==2)&(ii==i)&(jj==j-1)&(kk==1))
x=(j-(N/2+1))*a; y=(i-((N+1)/2))*a; theta=((2*pi)-atan(y/x));

phase=(complex(cos(theta),-sin(theta)));
t=((Delta)*(phase))/t0;

else if((i>=(N/2+1))&(j>=(N/2+1))&(k==1)&(ii==i+1)&(jj==j)&(kk==2))
x=(j-((N+1)/2))*a; y=(ii-(N/2+1))*a; theta=((2*pi)-atan(y/x));

phase=(complex(cos(theta),sin(theta)));
t=-((Delta)*(phase))/t0;

else if((i>=(N/2+1))&(j>=(N/2+1))&(k==2)&(ii==i+1)&(jj==j)&(kk==1))
x=(j-((N+1)/2))*a; y=(ii-(N/2+1))*a; theta=((2*pi)-atan(y/x));

phase=(complex(cos(theta),-sin(theta)));
t=-((Delta)*(phase))/t0;

else if((i>=(N/2+2))&(j>=(N/2+1))&(k==1)&(kk==2)&(jj==j)&(ii==i-1))
x=(j-((N+1)/2))*a; y=(i-(N/2+1))*a; theta=((2*pi)-atan(y/x));

phase=(complex(cos(theta),sin(theta)));
t=-((Delta)*(phase))/t0;

else if((i>=(N/2+2))&(j>=(N/2+1))&(k==2)&(kk==1)&(jj==j)&(ii==i-1))
x=(j-((N+1)/2))*a; y=(i-(N/2+1))*a; theta=((2*pi)-atan(y/x));

phase=(complex(cos(theta),-sin(theta)));
t=-((Delta)*(phase))/t0;

%-------------------------------------------------
%  theta is 2pi
%-------------------------------------------------

%-------------------------------------------------
%i==N/2 & j>=N/2 because we are looking for the phase difference 2pi
%-------------------------------------------------

else if((i==N/2)&(j>=(N/2+1))&(k==1)&(ii==(N/2+1))&(jj==j)&(kk==2))
theta=(2*pi);

phase=(complex(cos(theta),sin(theta)));
t=-((Delta)*(phase))/t0;
```

```
else if((i==N/2)&(j>=(N/2+1))&(k==2)&(ii==(N/2+1))&(jj==j)&(kk==1))
theta=(2*pi);

phase=(complex(cos(theta),-sin(theta)));
t=-((Delta)*(phase))/t0;

else if((i==(N/2+1))&(j>=(N/2+1))&(k==1)&(ii==N/2)&(jj==j)&(kk==2))
theta=(2*pi);

phase=(complex(cos(theta),sin(theta)));
t=-((Delta)*(phase))/t0;

else if((i==(N/2+1))&(j>=(N/2+1))&(k==2)&(ii==N/2)&(jj==j)&(kk==1))
theta=(2*pi);

phase=(complex(cos(theta),-sin(theta)));
t=-((Delta)*(phase))/t0;

%-------------------------------------------------------------
else
t=0;
end
end
end
end
end
end
end
end
end
end
end
end
end
end
end
end
end
end
end
end
end
end
end
end
```

```
end
end
end
end
end
end
end
end
end
end
end
end
end
end
end
end
end
end
end
end
end
end
end
end
end
end
end
end
end
end
end
end
end
end
if t ~=0
d(cnt)=I;
e(cnt)=II;
f(cnt)=t;
cnt=cnt+1;
end
end
end
end
end
end
end
i
end
```

```
%-----------------------------------------------------
% introducing the Hamiltonian matrix H
%-----------------------------------------------------

H=sparse(d,e,f);
Hn=H+0;

%-----------------------------------------------------
% solving the eigen value problem
%-----------------------------------------------------

E=eig(Hn);
E=E(E<0);

%-----------------------------------------------------
% finding the total energy
%-----------------------------------------------------

summ=sum(E);
```

Bibliography

[1] G. Burnes, *High-Temperature Superconductovity,*(Academic Press, Inc. 1992).

[2] M. Tinkham, *Introduction to superconductivity*, 2nd Edition(McGraw-Hill, Inc. 1996)

[3] A. C Rose-Innes and E. H Rhoderick, *Introduction to superconductivity*, 2nd Edition(Pergamon Press Ltd., Exeter, 1987)

[4] C. Kittel, *Introduction to Solid States Physics*, 7th Edition(John Wiley, Inc. 1996).

[5] G. Baskaran, Z. Zou, and P. W. Anderson, *Solid State Commun.* **63**, 973, 1987.

[6] Assa Auerbach, *Interacting Electrons and Quantum Magnetism*, (Springer-Verlag New York, Inc. 1994).

[7] P. G. De Gennes, *Superconductivity of Metals and Alloys*, (Perseus Book Publishing L.L.C. 1999)

[8] O. Vafek, A. Melikyan, and Z. Tesanovic, *Phys. Rev. B* **64**, 225408.

[9] O. Vafek, A. Melikyan, M. Franz, and Z. Tesanovic, *Phys. Rev. B* **63**, 135409.

[10] J. X. Zhu, T. K. Lee, C. S. Ting, and C. R. Hu, *Phys. Rev. B* **61**, 13, 2000.

[11] A.V. Balatsky, M.I. Salkola, and A. Rosengren, *Phys. Rev. B* **51**, 15, 547, 1995; A.V. Balatsky, and M.I. Salkola, *Phys. Rev. Lett.* **76**, 2386, 1996.

[12] S. H. Pan, E. W. Hudson, A. K. Gupta, K. W. Ng, H. Eiksi, S. Uchida, and J. C. Davis, *Phys. Rev. Lett.* **85**, 7, 2000.

[13] G. Binnig, H. Rohrer, C. Gerber, and E. Weibel, *Phys. Rev. Lett.* **49**, 5761, 1982.

[14] J. R. Waldram, *Superconductivity of Metals and Cuprates*, (Institute of Physics Publishing 1996)

[15] S. H. Pan, E.W. Hudson, and J. C. Davis, *Rev. Sci. Instruments* **70**, 1459, 1999.

[16] Q. H. Wang and D. H. Lee, *Phys. Rev. B* **67**, 020511, 2003.

[17] C. Caroli, P. G. DeGennes, and J. Matricon, *Phys. Rev. Lett.* **9**, 307, 1964.

[18] H. F. Hess, R. B. Robinson, R. C. Dynes, J. M. Valles, and J. V.Waszczak, *Phys. Rev. Lett.* **62**, 214, 1989.

[19] D. J. Griffiths, *Introduction to Quantum Mechanics* (Englewood Cliffs, New Jersey: Prentice-Hall, Inc., 1995), 1^{st} edition.

[20] P. I. Soininen, C. Kallin, and A. J. Berlinsky, *Phys. Rev. B* **50**, 13883, 1994.

[21] Y. Wang and A. H. MacDonald, *Phys. Rev. B* **52**, R3876, 1995.

[22] M. Ichioka, N. Hayashi, N. Enomoto, and K. Machida, *Phys. Rev. B* **53**, 15316, 1996.

[23] M. Franz and Z. Tesanovic, *Phys. Rev. Lett.* **80**, 4763, 1998.

[24] G. E. Volovik, *JETP Lett.* **58**, 469, 1993.

[25] C. Renner, B. Revaz, K. Kadowaki, I. Maggio-Aprile, and O. Fischer, *Phys. Rev. Lett.* **80**, 3606, 1998.

[26] I. Maggio-Aprile, C. Renner, A. Erb, E. Walker, and O. Fischer, *Phys. Rev. Lett* **75**, 2754, 1995.

[27] S. H. Pan, E. W. Hudson, K. M. Lang, H. Eisaki, S. Uchida, and J. C. Davis, *Nature* **403**, 746, 2000.

[28] R. E. Peierls, *Z. Physik* **80**, 763, 1933.

[29] Jian-Xin Zhu, T.K. Lee, C. S. Ting, and Chia-Ren Hu, *Phys. Rev. B* **61**, 8667, 2000.